The Astronomical Journal, 130:1733–1751, 2005 October

OPTICAL SPECTROSCOPY OF THE SURFACE POPULATION OF THE ρ OPHIUCHI MOLECULAR CLOUD: THE FIRST WAVE OF STAR FORMATION

Bruce A. Wilking
Department of Physics and Astronomy, University of Missouri—St. Louis, 1 University Boulevard, St. Louis, MO 63121; bwilking@umsl.edu

Michael R. Meyer
Steward Observatory, University of Arizona, Tucson, AZ 85721; mmeyer@gould.as.arizona.edu

John G. Robinson
Department of Physics and Astronomy, University of Missouri—St. Louis, 1 University Boulevard, St. Louis, MO 63121; johnr@newton.umsl.edu

and

Thomas P. Greene
NASA Ames Research Center, MS 245-6, Moffett Field, CA 94035-1000; tgreene@mail.arc.nasa.gov
Received 2004 December 14; accepted 2005 May 31

ABSTRACT

We present the results of optical spectroscopy of 139 stars obtained with the Hydra multiobject spectrograph. The objects extend over a 1.3 deg^2 area surrounding the main cloud of the ρ Oph complex. The objects were selected from narrowband images to have Hα in emission. Using the presence of strong Hα emission, lithium absorption, location in the Hertzsprung-Russell diagram, or previously reported X-ray emission, we were able to identify 88 objects as young stars associated with the cloud. Strong Hα emission was confirmed in 39 objects with line widths consistent with their origin in magnetospheric accretion columns. Two of the strongest emission-line objects are young, X-ray-emitting brown dwarf candidates with M8 spectral types. Comparisons of the bolometric luminosities and effective temperatures with theoretical models suggest a median age for this population of 2.1 Myr, which is significantly older than the ages derived for objects in the cloud core. It appears that these stars formed contemporaneously with low-mass stars in the Upper Scorpius subgroup, likely triggered by massive stars in the Upper Centaurus subgroup.

Key words: ISM: individual (ρ Ophiuchi cloud) — open clusters and associations: individual (Upper Scorpius) — stars: formation — stars: pre–main-sequence

Online material: machine-readable tables

1. INTRODUCTION

Nearby molecular clouds that are the sites of active star formation are observed to be surrounded by a population of less obscured and more evolved young stars. Hα emission-line and X-ray surveys have revealed large numbers of pre-main-sequence stars that extend well beyond the molecular cloud boundaries. For example, the *ROSAT* All-Sky Survey has led to the identification of 112 lithium-rich pre-main-sequence stars that are spread over a 450 deg^2 area surrounding the Orion star-forming molecular clouds (Alcalá et al. 1996). While some of the young stars appear to be related to earlier star formation in the Gould Belt, at least 60% are found to be directly associated with the Orion molecular cloud complex (Alcalá et al. 2000). Proposed origins for these associated young stars include formation in rapidly moving cloudlets that have since dispersed (Feigelson 1996) or ejection from the cloud core due to three-body encounters (Sterzik & Durisen 1995). Alternatively, they could simply be fossil tracers of previously existing dense molecular gas in analogy with OB associations and now-dispersed giant molecular clouds (e.g., Blaauw 1991). Clearly, determining the age and distribution of pre-main-sequence stars surrounding the denser molecular gas holds the key to describing the star formation history of a region and perhaps sets limits to the lifetime of the molecular cloud.

The ρ Oph cloud complex, located at the edge of the Upper Scorpius subgroup in the Sco-Cen OB association, is composed of a series of filamentary dark clouds that extend eastward from cores of dense molecular gas (de Geus 1992). At a distance of about 150 pc, it is one of the closest regions of active star formation. The main cloud, L1688, hosts a 1 pc $\times$ 2 pc centrally condensed molecular core in which the visual extinction is estimated to be 50–100 mag (Wilking & Lada 1983). The core of L1688 has been the focus of numerous near-infrared, far-infrared, and millimeter continuum surveys, as well as X-ray and radio continuum surveys, and is found to host an embedded infrared cluster with around 200 young stellar objects (YSOs; e.g., Greene & Young 1992; Bontemps et al. 2001; André & Montmerle 1994; Gagné et al. 2004). Infrared spectroscopic studies infer a median age of 0.3 Myr for objects in the core (Greene & Meyer 1995; Luhman & Rieke 1999). It has been suggested that star formation in the ρ Oph core is the latest in a chain of events that began with massive stars in the Upper Centaurus–Lupus and Lower Centaurus–Crux subgroups of the Sco-Cen OB association triggering the formation of OB stars in the Upper Scorpius subgroup, which in turn initiated star formation in the L1688 cloud (de Geus 1992).

Until recently, there has been limited study of the nature of lightly extincted association members at the periphery of the L1688 cloud that have been identified through Hα objective-prism and X-ray surveys (e.g., Dolidze & Arakelyan 1959; Wilking et al. 1987; Montmerle et al. 1983; Casanova et al. 1995). Early spectroscopic studies of Hα emission-line stars presented spectral types for about 20 young stars (Struve

& Rudkjøbing 1949; Cohen & Kuhi 1979; Rydgren 1980). An optical spectroscopic survey of ρ Oph X-ray sources was conducted by Bouvier & Appenzeller (1992) and established spectral types for 30 pre-main-sequence stars (23 new). They found an age of 1–10 Myr for these objects, significantly older than the age of objects in the core (see also Greene & Meyer 1995). But these samples favored the brighter association members and gave the incorrect impression that there was a deficiency of M-type stars relative to other nearby star-forming regions (see Fig. 24 of Hillenbrand 1997). This was remedied in part by Martín et al. (1998), who obtained optical spectroscopy for 59 *ROSAT*-selected sources in the core and streamer of the cloud with the majority of objects classified as pre-main-sequence M stars. By examining the ratio of classical T Tauri stars (CTTSs) to weak-emission T Tauri stars (WTTSs), they found evidence for an older pre-main-sequence population outside of the L1688 core.

In an effort to identify more widely distributed and/or older late-type association members, we have obtained deep narrowband images of a 1.3 deg^2 area encompassing the L1688 cloud and centered at the wavelengths of Hα and [S II]. Shorter exposures at *R* and *I* were also obtained. This resulted in a sample of 282 candidate CTTSs with $R < 20$ mag that had possible Hα emission. This sample includes association members with greater obscuration and/or lower mass than those targeted by previous surveys. Using the multiobject spectrograph Hydra, optical spectra were obtained for 129 candidate CTTSs plus 10 additional objects with $R < 19.1$ mag. Our sample selection procedure and the observations are described in § 2. In § 3, we detail our criteria for spectral classification and our examination of surface gravities. The results of the spectral classifications and an analysis of the emission-line spectra are given in § 4. Also in § 4, we list the criteria used to identify 88 association members from the sample and their locations in a Hertzsprung-Russell (H-R) diagram. In § 5, we compare the properties of the association members with those of low-mass stars in the Upper Scorpius subgroup of the Sco-Cen OB association to gain insight into the star formation history of the ρ Oph cloud.

2. OBSERVATIONS AND DATA REDUCTION

Moderate-resolution spectra were obtained for 129 of 282 stars identified as candidate CTTSs from narrowband Hα images of the ρ Oph cloud or from Hα objective-prism plates (Wilking et al. 1987). In addition, spectra were obtained for five bright association members and five brown dwarf candidates in the cloud not identified as candidate CTTSs. A total of 139 stars were observed. These observations are described in detail in the sections below.

2.1. *Sample Selection*

The majority of candidate CTTSs were selected from deep optical images of a 1.3 deg^2 area centered on the L1688 cloud obtained with the Curtis Schmidt telescope at Cerro Tololo Inter-American Observatory. The images were obtained on 1995 March 10, and their reduction is described elsewhere (Wilking et al. 1997). Briefly, long (45 minute) exposure narrowband images centered at the wavelengths of Hα (FWHM = 64 Å) and [S II] (FWHM = 45 Å) were obtained in addition to short (5 minute) exposures in the standard *R* and *I* bands. The latter were calibrated in the Johnson-Kron-Cousins photometric system using standard star fields established by Landolt (1992). The *R*- and/or *I*-band photometry was obtained for over 2700 stars in the Ophiuchus field with $R < 20$. Accurate positions ($<0\farcs5$) for these stars were obtained using the ASTROM program distributed by the Starlink Project and a set of secondary astrometric standards and then shifted by +0.2 s in right ascension to bring them into agreement with the Two Micron All Sky Survey (2MASS) coordinate system (Cutri et al. 2003). The narrowband images were used to estimate the equivalent width of possible Hα emission. The continuum in the Hα filter was estimated using the flux in the [S II] filter after correcting for the differences in filter widths and transmission and assuming a flat continuum with no [S II] emission. The latter assumption was shown to be valid, with detections of weak [S II] emission in only two sources. As a result, 282 stars with $R < 20$ were identified with possible Hα emission [EW(Hα) > 10 Å]. However, because of structure in the continuum due to reddening and photospheric absorption bands, it was desirable to confirm this emission spectroscopically.

2.2. *Hydra Observations*

We obtained 151 spectra for 139 stars located toward the cloud and its periphery on 1999 May 5–6 using Hydra, the multifiber spectrograph, on the WIYN 3.5 m telescope.[1] The Bench Spectrograph Camera was used with the red fiber cable, the 600 lines mm^{-1} grating with a blaze angle of $13\fdg9$, and the GG495 filter to cover the range of 5820–8700 Å centered near 7200 Å. The spectral dispersion was 1.39 Å pixel^{-1}, giving an effective resolution of 2.88 Å. The resolution at the central wavelength was $\lambda/\Delta\lambda = 2500$. The program objects were selected by *R* magnitude, the Hα equivalent width estimated from the narrowband images, and their accessibility to a fiber. Program objects were distributed among four fiber configurations sorted by *R* magnitude; 12 program stars were observed in two configurations. Field 1 included the brightest candidate CTTSs ($R < 15$) and, to make most efficient use of the spectrograph, five bright X-ray sources known to be association members but with no known Hα emission. Fields 2 and 3 sampled the same magnitude range of candidate CTTSs ($15 < R < 17$) with the pointing centers shifted in declination. Field 4 candidates ($17 < R < 19.1$) were supplemented by five brown dwarf candidates from the study of Wilking et al. (1999, hereafter WGM99). We observed 81% of the candidate CTTSs with $R < 15$, 88% of the candidates with $15 < R < 17$, 45% of the candidates with $17 < R < 18$, and 21% of the candidates with $17 < R < 19.1$. In Table 1 we summarize the observations by presenting for each field the pointing center, *R* magnitude range, number of candidate CTTSs observed, integration time, and number of exposures.

The spectra were reduced using the Image Reduction and Analysis Facility (IRAF).[2] Images were processed for bias and dark corrections using *ccdproc*. Multiple exposures of a given field were median-combined and then reduced with IRAF's *dohydra* package. The images were flat-fielded using dome flats obtained for each fiber configuration, except for field 1, in which the flat from the configuration for field 2 was used. Sky subtraction was accomplished using the median of 7–10 sky spectra distributed across each field. The spectra were wavelength-calibrated using 5 s exposures of CuAr lamps. Scattered-light corrections were not made, and no flux calibration was performed. It was necessary in a few cases to improve the sky subtraction by first

[1] The WIYN Observatory is a joint facility of the University of Wisconsin—Madison, Indiana University, Yale University, and the National Optical Astronomy Observatory (NOAO).

[2] IRAF is distributed by the NOAO for the Association of Universities for Research in Astronomy (AURA), Inc.

TABLE 1
Summary of Hydra Observations

Field Number	R.A. (J2000.0)	Decl. (J2000.0)	R (mag)	Sources Observed	Integration Time (s)	Number of Exposures	S/N[a]
1.....	16 27 09.5	−24 25 43.5	15	28	600	4	21
2.....	16 26 46.2	−24 11 45.0	15–17	30	1800	4	21
3.....	16 27 19.9	−24 41 42.8	15–17	35	1800	2	23
4.....	16 27 18.3	−24 23 42.9	17–19.1	58	1800	4	16

Note.—Units of right ascension are hours, minutes, and seconds, and units of declination are degrees, arcminutes, and arcseconds.
[a] Median of S/N computed from 7400 to 7500 Å.

scaling the median sky spectrum before subtracting it from the source spectrum. The typical signal-to-noise ratio (S/N) for the spectra extracted in each field is presented in Table 1.

3. ANALYSIS OF THE SPECTRA

Spectral types were derived from visual classification (visual pattern matching of our smoothed program-star spectra with standard-star spectra) supported by quantitative analysis of some spectral indices. In this section, we provide descriptions of the absorption lines used to classify three broad groups, starting with the earliest spectral type stars (B–A), moving to the F–K stars, and ending with the M stars. We conclude this section with a discussion of gravity-sensitive absorption features in the 5820–8700 Å spectral range. For the purposes of matching spectral features with those of standard stars, our Hydra spectra were smoothed using a Gaussian filter to the resolution of the standard stars for direct comparison. All spectra have been normalized to 1 by dividing out a fit to the continua, carefully excluding regions with emission lines or broad absorption due to TiO and VO. Normalized spectra smoothed to a resolution of 5.7 Å are shown in Figure 1 for a representative sample of program objects, with early-type stars in Figure 1*a* (B3–G9), K stars in Figure 1*b*, early- to mid-M stars in Figure 1*c*, and mid- to late-M stars in Figure 1*d*. Both photospheric and telluric spectral features are labeled.

Two main sets of standards were used for classification (both qualitative and quantitative). First, optical spectra from the WIYN Hydra study of the Praesepe by Allen & Strom (1995) were used to derive spectral types from B8 V to M4 V. The effective resolution of these spectra was 5.7 Å. For giants and later type dwarfs (M5 V–M9 V), optical spectra from the study of Kirkpatrick

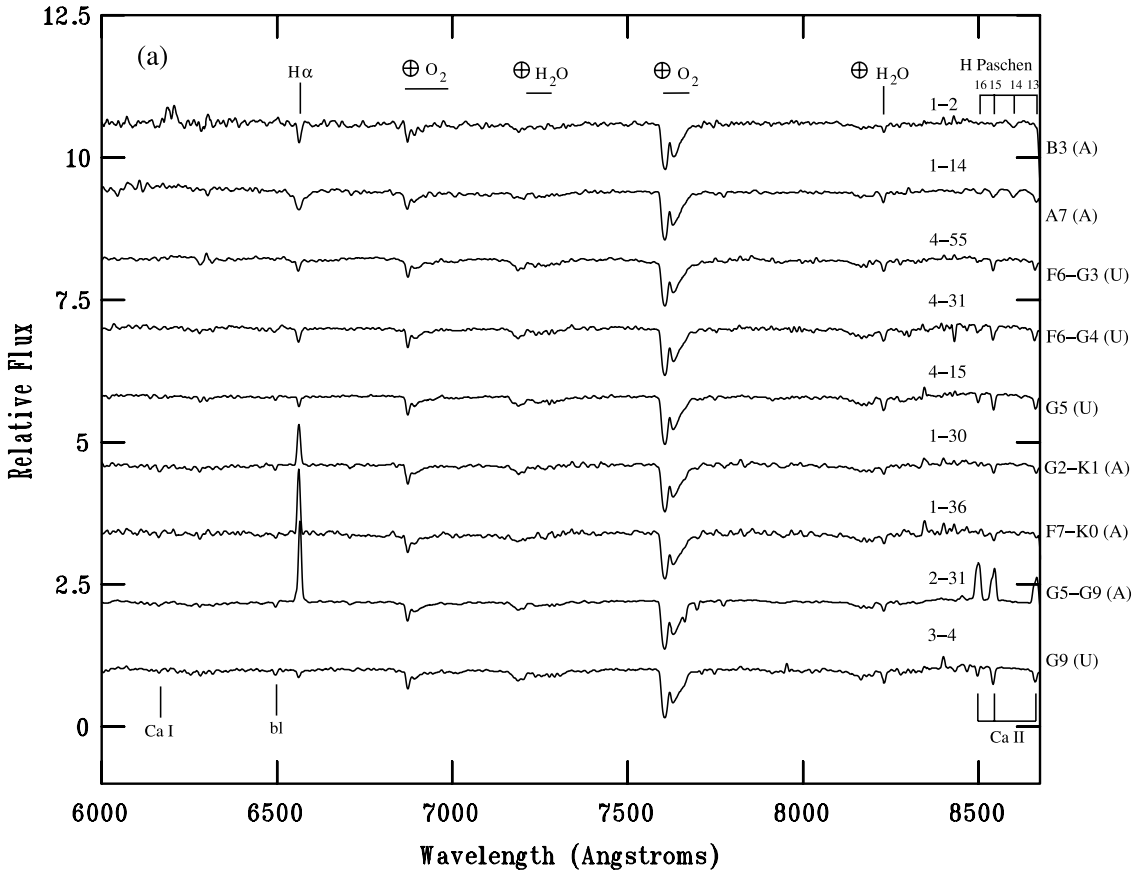

Fig. 1.—Collection of spectra representative of the entire sample, smoothed to a resolution of 5.73 Å and normalized using a polynomial fit. The spectra are labeled with their field and aperture numbers (Table 2) and a spectral type or range. In addition, an indicator of association membership (A) or undetermined (U) follows the spectral type. Atomic and molecular bands of interest in our classification scheme are labeled, as are telluric features. Shown are (*a*) B–G stars; (*b*) K stars; (*c*) early M stars; and (*d*) late M stars. Included in (*c*) and (*d*) are spectra of giants and dwarfs from our survey to illustrate the intermediate surface gravity of the YSOs.

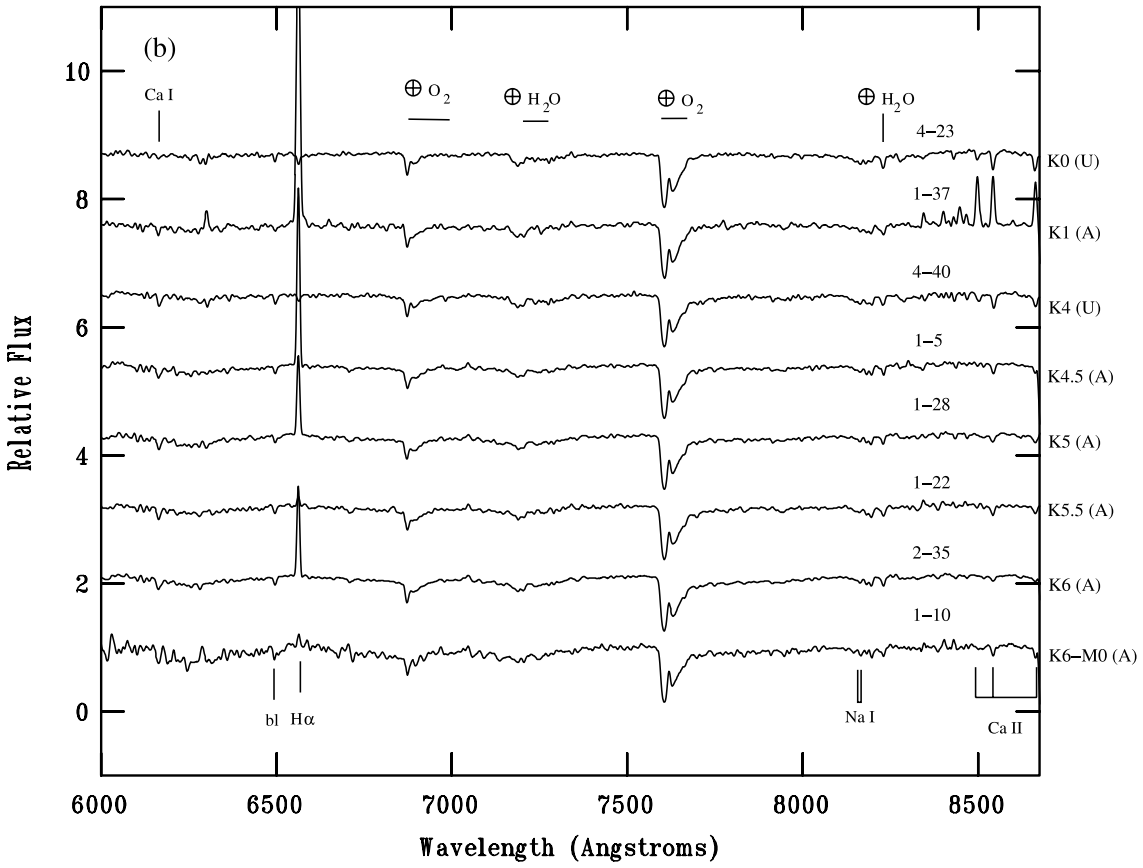

FIG. 1.—*Continued*

et al. (1991) were used with an effective resolution of either 8 or 18 Å. In addition to these, optical spectra of very late type subgiants in IC 348 (Luhman 1999) and ρ Oph (Luhman et al. 1997) were used for comparison with the coolest stars in our sample. For stars earlier than B8 V, we referred to the spectral atlas of Torres-Dodgen & Weaver (1993).

3.1. *Classification of B–A Stars*

Absorption lines from the Balmer ($n = 2$) and Paschen ($n = 3$) series of hydrogen are prominent in the spectra of early-type stars. In our spectra, we see unblended absorption lines from Hα (6563 Å) and Paschen 14 (8598 Å) (see Fig. 1*a*) that reach a maximum around A0 and weaken in warmer stars. The Ca II triplet (8498, 8542, 8662 Å) is also observed and decreases in strength toward early-type stars until overtaken by Pa 16, 15, and 13 (8502, 8545, and 8665 Å). Hence, an F2 star may have an EW(Hα) similar to that of a B5 star but will be distinct by displaying stronger absorption from the Ca II triplet. We note that all the aforementioned lines can appear in emission, and that the observed absorption-line strengths could be lower limits to the true strengths. We estimate that the uncertainty in our derived spectral types in this range is ± 5 subclasses; however, our adopted spectral types will be greatly aided by previously published observations of these intrinsically bright stars.

3.2. *Classification of F–K5 Stars*

The relative strength of absorption due to Hα and a blend of Ba II, Fe I, and Ca I centered at 6497 Å is the most sensitive indicator of spectral type over this range. Also helpful in spectral classification is absorption due to Ca I at 6122 Å, which grows stronger from spectral types A to K (e.g., compare Figs. 1*a* and 1*b*). Absorption from the Ca II triplet is present but shows little variation with spectral type in F–K stars. In general, the variation in these features is very gradual from subclass to subclass, and, when coupled with the S/N of the spectra, the uncertainties in the spectral classifications between F0 and K0 are often ± 3–5 subclasses. Paschen line absorption (13 and higher transitions) will be present through mid-F stars, but Pa 13, 15, and 16 are blended and dominated by the lines from the Ca II triplet at our resolution. Once again, the partial filling of Hα absorption by Hα emission in CTTSs could lead us to assign spectral types that are too late.

3.3. *Classification of K5–M9 Stars*

For stars K5 V and later, the depths of the TiO and VO bands provide the most sensitive indicators of spectral type. As shown in Figure 1*b*, TiO absorption bands begin to appear in mid-K stars centered at 6300, 6700, and 7140 Å and increase in strength through M6 V stars (Figs. 1*c* and 1*d*). Absorption due to TiO, which begins near the strong telluric O_2 band (oxygen *B* band; 7594–7685 Å) and extends to 7861 Å, is evident for spectral types of M1 V and later and is further strengthened by VO absorption from 7851 to 7973 Å in mid- to late-M stars (Fig. 1*d*). TiO absorption bands from 8432 to 8452 Å also appear for spectral types of M2 V and later and increase in strength through M9 V (Fig. 1*d*). For the coolest M stars (M6–M9), the depths of the TiO bands centered at 7140 and 7800 Å appear to decrease due to the depletion of TiO into grains (e.g., Allen 1995; Fig. 2*a* in this paper); VO absorption from 7334 to 7543 Å and from 7851 to 7973 Å then becomes a more reliable indicator of spectral type.

Spectral classification in this temperature range was accomplished through a combination of visual classification and quantitative analysis of TiO and VO indices, which we now describe.

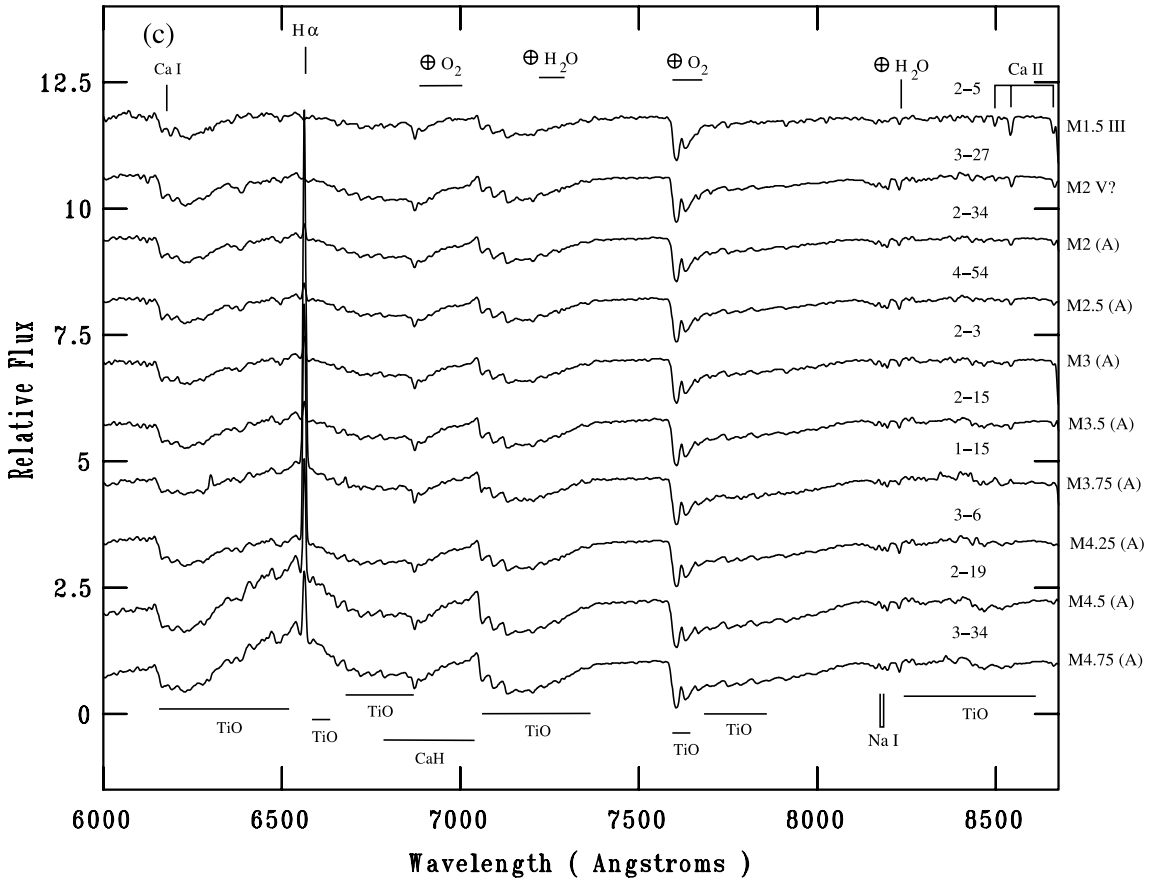

FIG. 1.—*Continued*

The indices were computed by taking the ratio of the average flux in a ~50 Å wide band of the continuum to the average in an absorption band. Following Allen (1995), we plotted the TiO index of the 7035 Å/7140 Å ratio versus the TiO index of the 7500 Å/7800 Å ratio along with their 1 σ errors for each Hydra field, as well as our dwarf standards. Figure 2*a* shows a plot of the TiO indices for the dwarf standards. There is a general trend for TiO index to increase with later spectral type until M7, at which the trend reverses and the index decreases for stars cooler than M7. To resolve the ambiguity caused by this reversal, we developed two narrowband VO indices for spectral classification of the coolest stars in our sample. A plot of these indices is shown in Figure 2*b* for M dwarf standards. The first index is the ratio of the continuum averaged over two bands that bracket the VO band centered at 7485 Å to the average flux in the VO band. The second index is the ratio of the continuum in a band centered at 8120 Å to the flux in the VO band centered at 7970 Å. As shown in Figure 2*b*, there is a general trend for the indices to increase from spectral types M3 to M9. While the use of these indices allowed us to sort objects by temperature, the final spectral classifications were made by direct comparisons of the strengths of the TiO and VO bands with standard-star spectra. The sensitivity of these absorption bands to spectral class allowed us in most cases to estimate M spectral types to within a subclass.

3.4. *Surface Gravities*

A rough estimate of the surface gravity of an object is important in determining its nature and accurately estimating its effective temperature for a given spectral type. In particular, surface gravity indicators can help identify background giants and field dwarfs that might contaminate our sample. Gravity-sensitive absorption features available for analysis in our spectra include the CaH band centered at 6975 Å and the Na I doublet at 8183, 8195 Å (both strongest in dwarfs) and absorption from the Ca II triplet at 8660 Å (strongest in giants). Of these features, CaH is well-positioned for study.

Following Allen (1995), we have calculated a CaH index as the ratio of the continuum at 7035 $\pm$ 15 Å to the flux in the CaH absorption band at 6975 $\pm$ 15 Å and a TiO index as the ratio of the continuum at 7030 $\pm$ 15 Å to the flux in the TiO absorption band at 7140 $\pm$ 15 Å from the normalized spectrum of each program object. In Figure 3, we plot the CaH index versus the TiO index for 136 program objects. Error bars are computed based on the 1 σ error in flux averages and propagated to the ratios. The solid lines represent first- or second-order fits to the standard-star spectra. Based on this plot, we conclude that the surface gravities for objects with the largest TiO index (coolest stars) are intermediate between those of giants and dwarfs. While there are clearly late-type giants present in our sample, about 70% of the program objects have TiO indices <2 (about spectral type M4 V) and surface gravities that most closely resemble dwarf stars. Therefore, spectral types for our program objects were determined by comparing them to a grid of dwarf standards.

4. RESULTS

Spectral types were determined for 131 of 139 stars in the manner described in § 3.3. Using the CaH index and other gravity-sensitive features (§ 3.4), six stars were identified as giants and 26 as possible dwarfs. These data are presented in

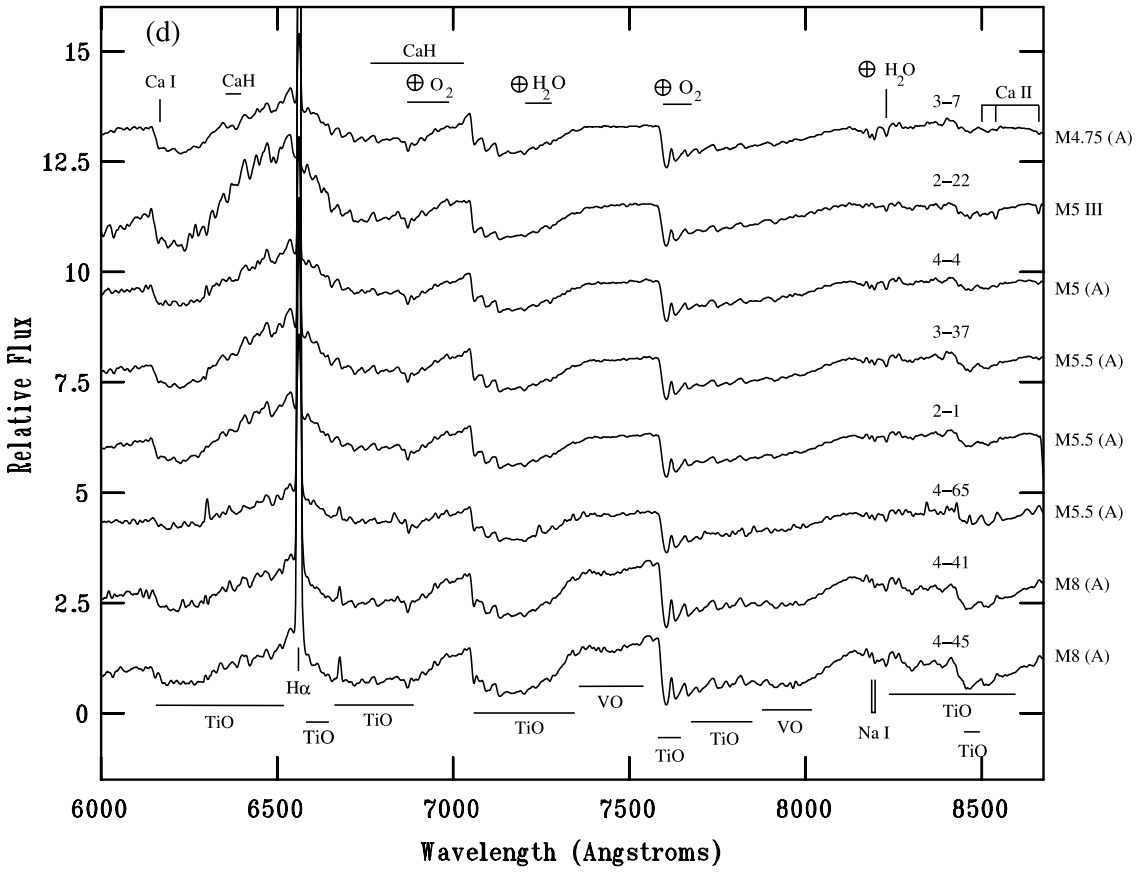

FIG. 1.—*Continued*

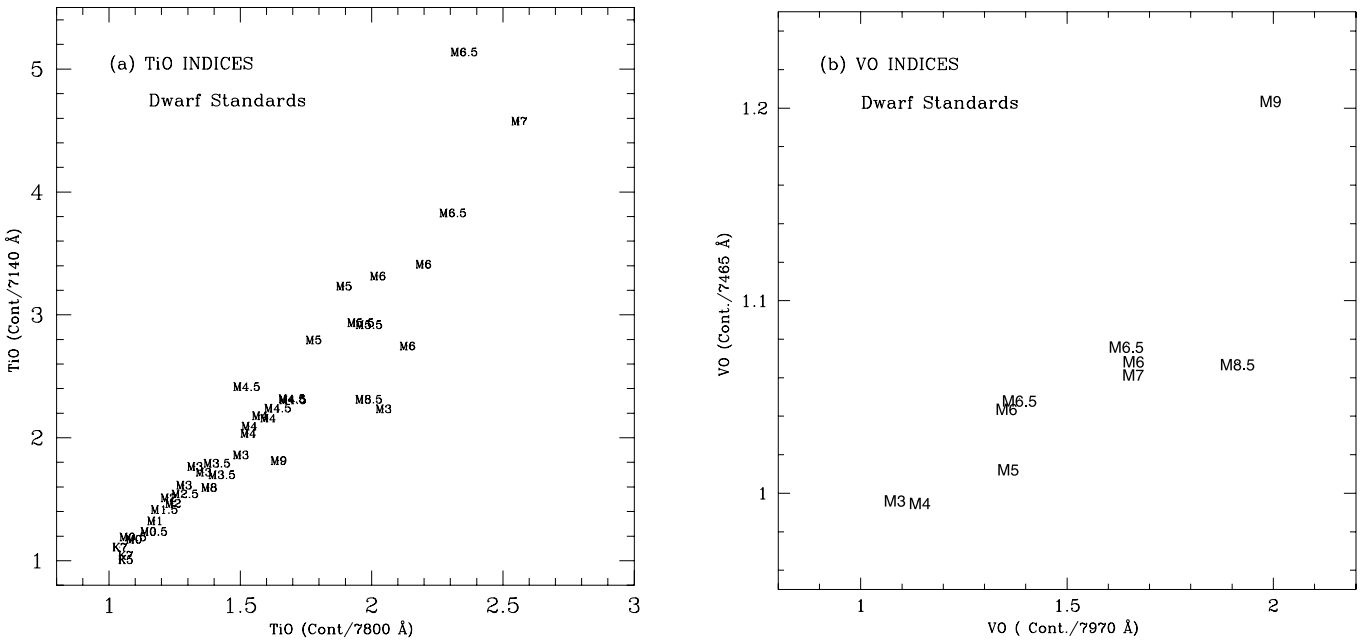

FIG. 2.—Spectral indices for dwarf standards used to guide our spectral classifications. Spectra from the studies of Allen & Strom (1995) or Kirkpatrick et al. (1991) were used in the analysis. (*a*) TiO index of the 7035 Å/7140 Å ratio vs. the TiO index of the 7500 Å/7800 Å ratio for K5–M9 dwarfs. The ratios were formed by averaging the flux in a 30 Å wide band centered on the wavelength. (*b*) Two VO band indices that are sensitive to spectral type for late M dwarf standard stars. The widths of the wavelength bands in the continuum were chosen to maximize the number of channels yet avoid strong absorption due to TiO. The *y*-axis shows the ratio of the continuum averaged between a 20 Å wide band centered at 7380 Å and a 30 Å wide band centered at 7555 Å to the flux in a 50 Å wide band centered in the VO band at 7465 Å. The *x*-axis shows the ratio of the continuum in a 40 Å wide band centered at 8120 Å to the flux in a 60 Å wide band centered in the VO band at 7970 Å.

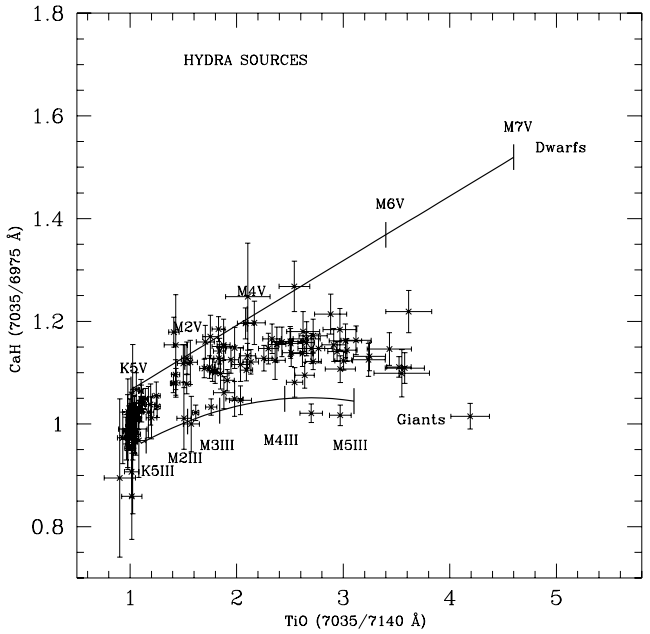

FIG. 3.—CaH vs. TiO indices as defined in the text for 136 program objects. The solid lines were derived from first- or second-order fits to dwarf and giant spectral standards. For the dwarf standards from K5 to M7, the fit was $y = 0.126x + 0.940$ with a correlation coefficient of $r = 0.94$. We note that for spectral types later than M7, both indices decrease so that an M8 V star has a CaH index similar to that of an M4 V star. For the giant standards from K5 to M5, the fit gave $y = -0.0357x^2 + 0.191x + 0.795$ with a correlation coefficient of $r = 0.82$.

Table 2, along with any previous source names, X-ray associations, right ascension and declination in J2000.0, and *R* and *I* magnitudes. The derived spectral types (or range of possible spectral types) are also shown to the right of each spectrum in Figure 1 along with its classification as a possible dwarf (V?), giant (III), association member (A), or association unknown (U). The top two spectra in Figures 1*c* and 1*d* demonstrate the different features present in high and low surface gravity objects of the same spectral type. In the following sections, we discuss what the spectra reveal about the characteristics of the young stars and their evolutionary states. Included in this discussion is the distribution of spectral types in our sample and the variety and properties of their emission lines. A description is given of how association membership was determined and the resulting spatial distribution of association members relative to the molecular gas. Finally, the evolutionary state of the population is estimated by deriving ages and masses using an H-R diagram.

4.1. *Distribution of Spectral Types*

The distribution of spectral types for our sample is shown in Figure 4. Over half (79) of the 131 objects with spectral-type determinations are M stars. The fact that our sample is dominated by M stars is due in part to a selection effect caused by the onset of TiO absorption bands. The procedure described in § 2.1 was designed to select objects with Hα emission provided the continuum was relatively flat. But the same procedure could erroneously identify M stars with strong TiO absorption as Hα emission-line objects, since the Hα filter bandpass lies in a spectral region free of TiO absorption, while the comparison [S II] filter bandpass lies within strong TiO absorption at 6700 Å.

The shaded areas of the histogram represent sources with strong Hα emission [EW(Hα) > 10 Å] at the time of our observations. Our procedure of selecting Hα emission-line stars from narrowband images was only moderately successful. In particular, our procedure appears to break down for the fainter sources ($R < 17$), which accounts for the number of background G stars in our spectroscopic sample. Our highest success rate occurred with mid-K stars and mid- to late-M stars and was 65%. In the latter group, Hα emission was clearly a factor in their identification in our original narrowband image. There is clearly no deficiency of M-type CTTSs in the ρ Oph cloud relative to other nearby star-forming regions. The apparent lack of M stars in previous spectroscopic surveys represents the bias toward brighter stars in those surveys.

4.2. *Emission-Line Spectra*

Nearly one-third of our sample for which we could determine spectral types displayed strong emission from Hα. The spectra for about one-third of these strong emitters also exhibited emission lines from He I, O I, Ca II, and/or Pa 14. Emission lines were identified, and their equivalent widths and FWHMs were measured using Gaussian fits. No attempt was made to deconvolve the emission profile by the instrument response. The results for all CTTSs are presented in Table 3.

Since our sample was based on a procedure designed to select sources with strong Hα emission characteristic of CTTSs, it is not surprising that 39 of the 131 objects with spectral-type determinations displayed strong Hα emission. Of these, 26 are newly identified CTTSs based on an EW(Hα) > 10 Å criteria. The previously identified CTTSs can be found in Table 2 by looking at sources with previously measured Hα emission (col. [10]). An additional 17 objects showed weaker Hα emission [10 Å > EW(Hα) > 5 Å], with nearly all having spectral types from M3 to M5. We note that variability plays a role in the identification of Hα emission (e.g., Wilking et al. 1987; Hartigan 1993). Among the six Hα emitters with multiple observations, the equivalent width of object 2-30 (field number and aperture from Table 2) dropped from 38 to 8.5 Å in only 1 day. The brown dwarf candidate GY 5 was observed to have an EW(Hα) = 15 Å, whereas a similar spectrum obtained in 1998 showed no detectable emission (WGM99). In addition, the shape of the emission profile also appeared to change in three cases (Chini 8, EL 24, and object 2-30). All the strong Hα emission lines were well-resolved with typical FWHMs of 250 km s^{-1} compared to the 128 km s^{-1} velocity resolution of our data.

These broad Hα profiles, which can exceed 300 km s^{-1} in our sample, have been successfully modeled as arising in magnetospheric accretion columns (Hartmann et al. 1994; Muzerolle et al. 2001). Thirteen of the Hα profiles were clearly asymmetric or displayed non-Gaussian wings. The profile shapes are noted in Table 3 using the classification scheme of Reipurth et al. (1996). The prevalence of wings or asymmetries on the blue side of the profile is typical among CTTSs and suggests the presence of mass outflows. The Ca II triplet at 8660 Å was observed in emission in 14 of the Hα emitters and was strongest in the G- or K-type objects. No attempt was made to deblend them from the weaker Paschen emission lines Pa 13, 15, and 16. In general, the Ca II lines were narrower than Hα and barely resolved in our data, with typical FWHMs of 150 km s^{-1}. Figure 5 shows an expanded view of the Hα emission and Ca II emission lines for a representative sample of seven CTTSs. As in Figure 1, the spectra have been smoothed to a resolution of 5.7 Å. Hα profiles for objects 1-24 and 1-29 were symmetric, while the rest of the profiles in Figure 5*a* exhibited a blueward asymmetry. Only the source object 2-31/1-35 (Figs. 5*a* and 5*b*, *bottom two spectra*) displayed asymmetric profiles in both Ca II and Hα.

TABLE 2

OPTICAL PROPERTIES OF CANDIDATE T TAURI STARS

Field[a] (1)	Aperture[a] (2)	Name(s)[b] (3)	X-Ray ID[c] (4)	R.A. (J2000.0) (5)	Decl. (J2000.0) (6)	CaH[d] (7)	TiO[e] (8)	EW(Li) (9)	Previous Hα[f] (Å) (10)	EW(Hα) (Å) (11)	I (mag) (12)	$(R-I)$ (mag) (13)	Previous Spectral Type[g] (14)	Spectral Type (15)	Adopted Spectral Type (16)	Notes (17)
2.....	15			16 24 57.3	−24 11 23.4	1.10	2.09	Yes	...	2.8	13.71	1.92	...	M3–4	M3.5	
2.....	22			16 25 01.5	−24 28 58.1	1.01	4.19	...	...	−0.10	13.85	2.42	...	M5	M5 III	Giant
2.....	14			16 25 24.1	−23 56 56.4	1.27	2.54	...	...	1.5	15.15	1.70	...	M2–4	M3	Dwarf?
2.....	10			16 25 24.3	−24 15 39.0	1.22	3.61	...	...	11	14.46	2.03	...	M5	M5	
1.....	7	SR 22, WSB 23	ROXRA2	16 25 24.4	−24 29 43.5	1.18	2.62	...	170	31	12.88	1.64	M3.5 (MMGC), M0 (LR)	M4.5	M4.5	[h]
2.....	13			16 25 28.8	−24 22 59.0	1.20	2.17	...	...	0.30	15.12	1.52	...	M3–3.5	M3.25	Dwarf?
3.....	27			16 25 29.9	−24 39 14.5	1.16	1.71	...	...	−0.10	14.15	1.22	...	M2	M2	Dwarf?
4.....	43			16 25 31.6	−24 21 21.6	0.98	1.02	...	...	−0.50	17.02	1.62	...	K0–3	K1.5	
2.....	8			16 25 37.8	−24 13 43.1	1.02	2.97	Yes:	...	0.40	13.56	2.47	...	M4–4.5	M4.25 III	Giant
3.....	15	WLY 2-3	ROXRA4	16 25 39.6	−24 26 34.0	1.10	1.43	...	...	34	14.84	1.94	...	M2	M2	
2.....	32		ROXR1-7	16 25 47.7	−24 37 38.7	1.13	2.26	Yes	4.9	4.7	14.25	1.92	M4 (MMGC)	M3–4	M3.5	
1.....	22	VSS 23, WLY 2-10	ROXRA5	16 25 50.5	−24 39 13.9	1.03	1.08	Yes:	2.5	1.2	12.37	1.45	K2 (BA)	K5–6	K5.5	Dwarf?
4.....	55			16 25 52.5	−24 04 18.7	1.02	1.01	...	...	−1.1	16.00	1.12	...	F6–G3	F9.5	
2.....	25	WLY 2-11	ROXC J162556.0	16 25 56.1	−24 30 14.4	1.15	3.06	...	...	12	14.52	2.28	...	M5	M5	6 cm[i]
3.....	18	Same as 2-25				1.14	3.02	...	...	14	...	...	...	...	...	
1.....	29	SR 4, WSB 25	ROXRA6	16 25 56.2	−24 20 47.5	1.03	1.05	Yes	87/220	67	11.33	0.63	K6 (BA), K8 (LR)	K4–5	K4.5	Ca em[j]
1.....	38	GSS 20	ROXRA7	16 25 57.5	−24 30 30.9	0.98	1.05	...	1.5	0.50	13.00	1.59	K7 (BA), K6 (LR)	K5–6	K5.5	Dwarf?
3.....	14			16 25 58.9	−24 52 47.4	1.17	2.72	Yes	...	4.7	13.84	1.93	...	M4.5	M4.5	Dwarf?
2.....	1	Chini 8	ROXRA8	16 25 59.6	−24 21 21.6	1.12	3.50	Yes	...	10	13.00	2.03	M4 (LR)	M5.5	M5.5	
3.....	24	Same as 2-1				1.11	3.56	Yes	...	10	...	...	...	...	...	
4.....	28		ROXRA9	16 26 01.6	−24 29 44.2	1.09	1.91	Yes:	...	3.0	15.00	2.22	...	M3	M3	
1.....	13	VSSG 19	ROXRA12	16 26 03.3	−24 17 46.0	1.17	1.75	...	2.1	2.1	12.99	1.71	M3 (MMGC)	M2	M2	
2.....	19			16 26 05.5	−23 55 40.7	1.15	2.91	Yes	...	11	13.75	2.10	...	M4.5	M4.5	
1.....	5	GSS 28, WSB 27	ROXRA15	16 26 17.1	−24 20 21.2	1.01	1.06	Yes	20	29	11.84	1.00	K5 (BA), M0 (LR)	K4–5	K4.5	
4.....	39			16 26 18.7	−24 07 18.7	1.13	2.10	Yes	...	2.3	13.06	1.80	...	M3–4	M3.5	
2.....	11		ROXR1-20	16 26 19.5	−24 37 26.8	1.15	2.97	Yes	4.8	4.0	13.31	1.85	M4.5 (MMGC)	M4.5–5	M4.75	
3.....	28	Same as 2-11				1.13	2.91	Yes	...	5.0	...	...	...	...	...	
3.....	26			16 26 21.1	−25 03 47.9	...	...	...	...	2.7	...	...	...	U	...	$R = 16.21$
1.....	25	WSB 28	ROXRA16	16 26 21.0	−24 08 51.4	1.12	1.57	...	...	10	13.08	1.62	...	M2	M2	
4.....	16	GY 5	ROXR1-C14	16 26 21.5	−24 26 00.4	1.10	3.55	...	...	15	15.80	2.50	M6 (WGM), M6 (N02)	M5.5	M5.5	
4.....	41	GY 3	ROXR1-21	16 26 21.9	−24 44 39.4	1.11	2.97	...	...	140	15.62	2.33	M7.5 (N02)	M8	M8	Ca em[j]
4.....	40			16 26 22.5	−23 58 19.2	1.03	1.04	...	...	−0.70	16.09	1.34	...	K3–K5	K4	
1.....	30	GSS 31, WSB 30	ROXRA18	16 26 23.3	−24 20 59.1	1.00	1.01	...	5	7.1	11.75	1.28	K0 (BA), K1 (LR)	G2–K1	G6	
1.....	28	DoAr 25, WSB 29	ROXRF1	16 26 23.7	−24 43 13.3	1.03	1.11	Yes	16	12	11.59	1.06	K7 (MMGC), K6 (LR)	K5	K5	
2.....	27	EL 24, WSB 31	ROXRA20	16 26 24.1	−24 16 13.0	1.02	1.05	Yes:	...	44	13.97	1.84	...	K5–6	K5.5	Ca em[j]
3.....	25	Same as 2-27				1.02	1.07	Yes:	...	50	...	...	...	...	...	
4.....	18			16 26 24.3	−24 01 15.6	1.18	2.97	...	...	8.0	15.83	2.12	...	M4.5	M4.5	Dwarf?
4.....	25		GDS J162625.7	16 26 25.7	−24 14 27.1	1.15	3.43	...	...	7.2	15.79	2.27	...	M5.5	M5.5	
4.....	66	GY 37	ROXR1-C15	16 26 27.9	−24 26 41.6	1.00	1.57	...	...	10	17.85	2.45	M6 (WGM)	M4.5–5.5	M5	
4.....	31			16 26 29.2	−24 48 16.0	1.00	0.99	...	...	−2.7	16.45	1.06	...	F6–G4	G0	
4.....	27	GY 59	GDS J162631.3	16 26 31.4	−24 25 30.6	...	...	...	...	0.0	18.90	...	M5 (LR), M6 (WGM)	M2–M5.5	M3.75	
2.....	36	WSB 34		16 26 33.0	−24 00 16.5	1.14	2.51	Yes:	...	51	14.13	1.89	...	M4.5	M4.5	
1.....	2	Source 1	ROXRA21	16 26 34.2	−24 23 27.8	1.02	1.04	...	−3.5	−2.6	12.57	1.95	B2 (CK), B4: (BA)	<B8	B3	6 cm[i]
4.....	4		ROXRA22	16 26 37.1	−24 15 59.4	1.16	3.12	Yes:	...	14	15.51	2.21	...	M5	M5	
2.....	29	WSB 37		16 26 41.3	−24 40 17.6	1.12	3.10	Yes	...	22	13.37	2.04	M4 (LR)	M5	M5	

TABLE 2—*Continued*

Field[a] (1)	Aperture[a] (2)	Name(s)[b] (3)	X-Ray ID[c] (4)	R.A. (J2000.0) (5)	Decl. (J2000.0) (6)	CaH[d] (7)	TiO[e] (8)	EW(Li) (9)	Previous Hα[f] (Å) (10)	EW(Hα) (Å) (11)	I (mag) (12)	$(R-I)$ (mag) (13)	Previous Spectral Type[g] (14)	Spectral Type (15)	Adopted Spectral Type (16)	Notes (17)
3.....	3	Same as 2-29				1.12	2.90	Yes	...	25	...	...	...	...	...	
4.....	11	GY 107		16 26 42.5	−24 22 17.1	...	...	...	...	0.0	...	...	M3 III (WGM)	U	...	
1.....	21		ROXC J162643.2	16 26 43.1	−24 11 09.1	1.01	1.20	...	...	0.70	13.30	1.53	...	K7–M0	K8	
1.....	20	GY 112	ROXRF2	16 26 44.3	−24 43 13.5	1.06	1.88	...	7.8	6.0	13.22	1.75	M3.5 (MMGC)	M2–4	M3	
3.....	22		ROXN6	16 26 44.4	−24 47 13.3	1.16	2.51	Yes	...	3.5	13.88	1.84	...	M4.5	M4.5	Dwarf?
4.....	13			16 26 46.1	−23 58 10.1	1.16	2.42	Yes	...	2.8	15.52	2.11	...	M2–4	M3	
1.....	36	WSB 38	ROXRA24	16 26 46.5	−24 11 59.7	0.97	1.04	Yes	19	10	12.37	1.53	G9: (BA), K8 (LR)	F7–K0	G3.5	
4.....	30		ROXRF3	16 26 47.1	−24 44 29.1	1.15	2.70	Yes	...	5.4	15.19	2.22	...	M4.5	M4.5	Dwarf?
4.....	59			16 26 48.2	−24 42 03.2	1.05	1.98	...	...	1.0	15.56	2.25	...	M3–4.5	M3.75	
1.....	32	WSB 40		16 26 48.6	−23 56 34.3	1.06	1.25	...	...	23	12.92	1.53	...	K5–6	K5.5	Ca em[j]
4.....	53	WL 18	ROXCH3	16 26 49.0	−24 38 24.8	0.97	1.08	...	...	96	17.38	1.95	...	K5–K8	K6.5	Ca em[j]
2.....	38			16 26 50.5	−24 13 51.9	1.16	2.50	...	...	5.5	14.78	2.04	...	M4.5	M4.5	Dwarf?
2.....	17			16 26 51.7	−24 03 53.9	1.02	2.70	...	...	0.10	13.11	2.36	...	M4	M4 III	Giant
4.....	32			16 26 53.2	−24 05 58.2	1.02	1.00	...	...	−1.9	16.88	1.52	...	G9–K2	K0.5	
2.....	9			16 26 55.0	−24 10 16.5	1.20	2.08	...	...	−0.40	13.81	1.47	...	M2–4	M3	Dwarf?
4.....	46		ROXC J162656.7	16 26 56.7	−24 13 51.2	1.02	1.17	...	...	14	16.29	2.17	...	K5–M0	K7	
4.....	26			16 26 57.8	−24 52 37.1	0.98	1.04	...	...	−0.20	17.45	1.01	...	K5	K5	Dwarf?
1.....	37	SR 24s, WSB 42	ROXRF7	16 26 58.5	−24 45 36.4	1.00	1.04	...	76	50	12.87	1.28	K7 (MMGC), K2 (LR)	K0–2	K1	Ca em[j]
4.....	42			16 26 59.1	−23 56 39.0	0.99	0.98	...	...	0.50	15.95	1.26	...	U	...	
4.....	63			16 27 06.6	−24 07 02.9	1.15	2.77	...	...	5.7	15.34	2.19	...	M4.5	M4.5	Dwarf?
4.....	65	GY 204	ROXCH17	16 27 06.7	−24 41 48.8	1.08	2.54	...	...	43	15.43	2.14	M6 (N02)	M5.5	M5.5	Ca em[j]
4.....	37			16 27 09.1	−24 12 00.6	1.10	1.85	...	...	4.0	16.14	2.33	...	M2–3	M2.5	
3.....	44	ROX 20a, WSB 45	ROXN27	16 27 14.5	−24 51 33.4	1.17	2.33	Yes	3	3.6	13.31	1.65	M5 (BA), M1–4 (LR)	M4.5	M4.5	Dwarf?
1.....	9	ROX 20b, WSB 46	ROXRF14	16 27 15.1	−24 51 38.5	1.13	1.53	Yes:	6.3	5.0	12.26	1.26	M2 (BA), M0–3 (LR)	M2	M2	Dwarf?
3.....	17	WSB 47		16 27 17.0	−24 47 10.9	1.01	1.08	...	...	−1.1	15.06	1.78	...	K0–2	K1	
4.....	10			16 27 17.5	−24 05 13.4	1.08	1.53	...	...	95	15.47	2.20	...	M3–4	M3.5	Ca em[j]
4.....	9			16 27 18.1	−24 53 16.5	1.15	1.88	...	...	1.0	16.63	2.02	...	M2–3	M2.5	Dwarf?
1.....	6	WSB 48		16 27 18.4	−24 54 52.5	1.25	2.10	...	...	90	13.23	1.47	...	M3–4.5	M3.75	
...	...	SR 12	ROXCH40	16 27 19.7	−24 41 39.9	...	...	...	4.5/8.8	...	11.10	1.30	K4/M2.5 (BA), M0 (LR)	...	M0	6 cm[i]
4.....	62			16 27 20.4	−23 58 42.5	0.91	1.01	...	...	−0.20	17.42	1.31	...	U	...	
3.....	6	WSB 49	ROXRF19	16 27 23.0	−24 48 06.8	1.12	2.13	Yes	...	37	13.31	1.75	...	M4–4.5	M4.25	
4.....	45	GY 264	ROXCH52	16 27 26.6	−24 25 54.2	1.12	3.24	...	...	155	15.72	2.18	...	M8	M8	Ca em[j]
3.....	7		ROXRF24	16 27 28.8	−24 54 31.4	1.21	2.88	...	...	8.0	14.32	1.70	...	M4.5–5	M4.75	Dwarf?
2.....	20		ROXR1-48	16 27 30.5	−24 32 34.7	1.19	1.83	...	...	−0.10	14.30	1.34	...	M2	M2	Dwarf?
3.....	33	Same as 2-20				1.18	1.83	...	...	−0.20	...	...	...	...	...	
4.....	22	GY 284	ROXR1-C27	16 27 30.9	−24 24 56.1	1.12	2.04	...	...	2.9	16.24	2.21	M1.5 (LR)	M3–3.5	M3.25	
4.....	12			16 27 31.0	−24 03 44.1	0.99	1.02	...	...	−0.30	17.63	1.13	...	U	...	
1.....	19			16 27 31.3	−23 59 08.7	1.18	1.41	...	...	0.10	13.12	1.02	...	M1	M1	Dwarf?
2.....	6	GY 295, WSB 50	ROXCH70	16 27 35.3	−24 38 33.4	1.14	2.77	Yes	...	4.2	14.08	2.08	M4 (LR)	M4.5	M4.5	
3.....	41	Same as 2-6				1.11	2.66	Yes	...	4.0	...	...	...	...	...	
1.....	1	GY 297		16 27 36.5	−24 28 33.3	1.12	1.50	...	...	−0.27	13.30	1.37	M0–3 (LR)	M2	M2	Dwarf?
4.....	54			16 27 38.0	−23 57 24.1	1.11	1.74	Yes	...	3.0	13.71	1.74	...	M2–3	M2.5	
2.....	35	DoAr 32, WSB 51	ROX 30b	16 27 38.3	−23 57 32.7	1.04	1.12	Yes	22	13	12.30	1.36	K4 (BA)	K5–7	K6	
4.....	24	WLY 2-49	ROXRF29	16 27 38.3	−24 36 58.4	1.05	1.11	...	...	20	15.52	2.17	K8 (LR)	K5–6	K5.5	
4.....	38	GY 310	ROXCH76	16 27 38.6	−24 38 38.4	0.79	1.70	...	...	0.0	17.40	...	M6 (N02), M8.5 (WGM)	M3–5	M4	
1.....	31	WSB 53		16 27 39.0	−23 58 18.9	1.06	1.10	Yes:	14	18	12.02	1.22	K4 (BA)	K5–6	K5.5	
3.....	5	GY 314, WSB 52	ROXRF30	16 27 39.5	−24 39 15.6	1.05	1.14	Yes	30	39	14.03	1.73	M0 (LR, MMGC)	K5	K5	Ca em,[j] 6 cm[i]

TABLE 2—*Continued*

Field[a] (1)	Aperture[a] (2)	Name(s)[b] (3)	X-Ray ID[c] (4)	R.A. (J2000.0) (5)	Decl. (J2000.0) (6)	CaH[d] (7)	TiO[e] (8)	EW(Li) (9)	Previous Hα[f] (Å) (10)	EW(Hα) (Å) (11)	I (mag) (12)	$(R-I)$ (mag) (13)	Previous Spectral Type[g] (14)	Spectral Type (15)	Adopted Spectral Type (16)	Notes (17)
1.....	26	SR 9, WSB 54	ROXRF31	16 27 40.3	−24 22 04.1	1.03	1.09	Yes	10.5/14	23	11.26	0.50	K5 (BA), K8 (LR)	K5	K5	
2.....	34		ROXC J162741.8	16 27 41.8	−24 04 27.3	1.13	1.83	Yes:	...	2.5	13.39	1.82	...	M2	M2	Dwarf?
4.....	64	GY 326	ROXCH81	16 27 42.7	−24 38 51.0	1.01	1.51	...	...	0.20	17.30	...	M4 (WGM)	M2	M2	
3.....	21			16 27 45.2	−25 03 32.7	1.17	2.66	Yes	...	3.5	14.09	1.83	...	M4.5	M4.5	Dwarf?
4.....	47			16 27 49.3	−23 56 09.0	1.02	1.01	...	...	0.0	16.48	1.06	...	F6–G9	G2.5	
1.....	14	VSSG 14	ROXR1-53	16 27 49.9	−24 25 40.3	0.98	0.98	...	−9.1	−8.0	12.19	1.50	A7 (GM, MMGC)	<F1	A7	6 cm[i]
1.....	10	ROX 31	ROXRF33	16 27 52.1	−24 40 50.3	1.04	1.19	...	3.3	1.3	12.66	1.60	K7 (BA)	K6–M0	K7.5	6 cm[i]
1.....	24	SR 10, WSB 57	ROXR1-C12	16 27 55.6	−24 26 18.0	1.11	1.70	Yes:	43	56	11.95	1.18	M1.5 (CK), M0 (LR)	M2	M2	Ca em[j]
4.....	8			16 27 59.7	−23 57 16.5	1.15	1.43	...	...	0.60	16.99	1.76	...	M0	M0	
3.....	34	WSB 58	ROXRF34	16 28 00.0	−24 48 19.3	1.14	2.62	Yes:	...	7.5	13.40	1.98	...	M4.5–5	M4.75	
3.....	31		ROXRF35	16 28 00.1	−24 53 42.5	1.13	3.25	Yes	...	14	13.51	2.05	...	M5	M5	
2.....	3			16 28 00.8	−24 00 52.0	1.10	1.77	Yes	...	3.2	13.89	1.85	...	M2–4	M3	
4.....	61			16 28 04.9	−23 56 08.4	0.97	0.97	...	...	−0.10	17.26	1.23	...	K5	K5	
4.....	5			16 28 09.9	−24 48 47.5	1.00	1.03	...	...	−0.80	16.66	0.88	...	K4–5	K4.5	
2.....	21			16 28 11.1	−24 06 17.9	1.16	2.38	Yes:	...	7.7	14.27	2.13	...	M3–4.5	M3.75	
3.....	13			16 28 11.3	−24 59 05.8	1.02	0.99	...	...	−1.5	15.90	1.00	...	G5–G9	G7	
3.....	11		ROXRF36	16 28 12.4	−24 50 44.9	1.15	1.88	Yes	...	6.0	13.67	1.93	...	M2–4	M3	Dwarf?
4.....	51			16 28 14.4	−23 57 52.1	1.01	1.01	...	...	0.0	17.49	1.18	...	G5–9	G7	
3.....	9			16 28 15.1	−25 02 07.3	1.03	1.02	...	...	−1.5	15.32	0.92	...	G9–K0	G9.5	
3.....	19			16 28 15.6	−25 03 49.5	1.00	1.02	...	...	−0.40	15.53	0.47	...	G9–K1	K0	
3.....	20	WSB 60		16 28 16.6	−24 36 58.3	1.09	2.64	Yes:	...	81	14.46	2.09	K8 (LR)	M4.5	M4.5	Ca em[j]
4.....	58			16 28 16.6	−24 07 36.4	1.07	1.06	...	...	0.0	16.77	1.69	...	U	...	
4.....	14			16 28 18.1	−23 57 30.4	1.00	1.01	...	...	−1.5	16.57	1.08	...	F6–G4	G0	
3.....	12			16 28 19.2	−24 57 34.2	1.15	1.98	Yes:	...	4.9	13.54	1.67	...	M2–4	M3	Dwarf?
2.....	12			16 28 20.0	−24 26 10.9	0.97	0.93	...	...	−0.80	15.69	1.21	...	F9–G9	G5	
4.....	3			16 28 20.1	−24 23 17.8	1.15	2.30	Yes:	...	4.1	15.55	2.14	...	M3–4	M3.5	
2.....	37		ROXC J162821.5	16 28 21.6	−24 21 55.2	1.14	1.48	...	...	1.0	14.95	2.02	...	M2–3	M2.5	
3.....	35	Same as 2-37				1.14	1.84	Yes:	...	3.0	...	...	...	...	...	
2.....	5			16 28 23.3	−24 18 34.3	1.03	1.59	...	...	−0.80	14.38	2.04	...	M1–2	M1.5 III	Giant
3.....	29	Same as 2-5				1.02	1.65	...	...	−1.0	...	...	...	...	...	
2.....	30		ROXC J162823.4	16 28 23.4	−24 22 40.6	1.03	1.02	...	...	35	14.60	1.69	...	K5	K5	Var Hα
3.....	42	Same as 2-30				1.02	1.05	Yes:	...	8.5	...	...	...	...	...	
2.....	4		ROXC J162824.2	16 28 24.3	−24 09 31.9	1.08	1.43	...	...	2.4	14.60	1.92	...	M2	M2	Dwarf?
3.....	39			16 28 24.9	−24 35 43.4	1.16	3.02	Yes	...	6.0	14.79	1.99	...	M5	M5	
1.....	11			16 28 25.1	−24 28 20.1	1.05	2.04	...	...	−0.50	12.46	1.79	...	M2	M2 III	Giant
4.....	44			16 28 28.3	−23 58 51.0	0.90	0.90	...	...	−0.20	17.17	1.20	...	U	...	
3.....	2			16 28 28.3	−24 52 21.6	1.03	1.26	...	...	−0.80	15.05	1.35	...	K6	K6	
4.....	23			16 28 29.4	−24 31 20.9	0.99	0.99	...	...	−0.90	16.56	1.22	...	K0	K0	
4.....	57			16 28 32.6	−24 15 24.1	1.12	2.36	...	...	4.0	15.95	2.35	...	M3–4	M3.5	
1.....	35	SR 20, WSB 61	ROX 33	16 28 32.7	−24 22 45.2	1.00	1.00	Yes:	21	15	11.36	1.23	G0: (BA), K8 (LR)	G5–9	G7	db Ca em[j]
2.....	31	Same as 1-35				1.00	1.00	Yes:	...	15	...	...	...	...	...	
4.....	50			16 28 36.3	−24 00 43.2	0.99	1.00	...	...	−1.2	16.28	1.57	...	K0–2	K1	
2.....	23		ROXC J162843.1	16 28 43.1	−24 22 52.3	1.16	2.62	...	...	6.4	14.47	2.07	...	M4.5–5	M4.75	[k]
3.....	1	Same as 2-23				1.16	2.69	Yes	...	6.0	...	...	...	...	...	
4.....	1			16 28 43.6	−24 04 44.7	1.00	0.99	...	...	−2.5	15.75	1.27	...	F7–G3	G0	
1.....	15	SR 13, WSB 62	ROX 34	16 28 45.3	−24 28 19.0	1.10	1.80	Yes:	30/48	46	10.95	1.45	M2.5 (BA)	M3–4.5	M3.75	Ca em[j]
4.....	49			16 28 47.0	−24 32 52.6	0.98	1.00	...	...	−1.20	16.85	1.10	...	G5–9	G7	

TABLE 2—*Continued*

Field[a] (1)	Aperture[a] (2)	Name(s)[b] (3)	X-Ray ID[c] (4)	R.A. (J2000.0) (5)	Decl. (J2000.0) (6)	CaH[d] (7)	TiO[e] (8)	EW(Li) (9)	Previous Hα[f] (Å) (10)	EW(Hα) (Å) (11)	I (mag) (12)	$(R-I)$ (mag) (13)	Previous Spectral Type[g] (14)	Spectral Type (15)	Adopted Spectral Type (16)	Notes (17)
3.....	43	WSB 63	ROXC J162854.0	16 28 54.1	−24 47 44.7	1.08	1.41	Yes	...	50	13.54	1.70	...	M1–2	M1.5	
4.....	56			16 28 59.2	−24 05 15.6	0.95	0.98	...	...	−1.9	17.04	0.78	...	F6–G9	G2.5	
3.....	4			16 29 00.0	−24 26 39.2	1.01	1.00	...	...	−1.1	15.20	1.00	...	G9	G9	
4.....	52			16 29 02.0	−24 31 10.7	0.98	0.99	...	...	−0.90	17.39	0.91	...	G5–K0	G7.5	
4.....	35			16 29 03.8	−24 30 2.4	1.13	1.95	...	...	−0.50	16.54	1.71	...	M2–4	M3	Dwarf?
3.....	37			16 29 04.0	−24 51 42.0	1.11	3.58	Yes	...	9.0	14.49	2.04	...	M5.5	M5.5	
4.....	20			16 29 11.6	−24 22 14.8	0.99	1.03	...	...	−1.1	17.80	1.09	...	F6–G5	G0.5	
1.....	3			16 29 12.7	−24 23 55.8	1.03	1.76	...	...	−1.1	11.68	...	...	M1–2	M1.5 III	Giant
4.....	60			16 29 21.1	−24 21 32.2	0.86	1.02	...	...	−0.10	17.70	0.96	...	U	...	
4.....	21			16 29 23.5	−24 27 51.2	0.98	0.99	...	...	−1.4	17.48	0.87	...	K0–2	K1	
4.....	15			16 29 23.9	−24 29 10.8	0.99	0.98	...	...	−1.4	16.11	1.02	...	G5	G5	
4.....	2			16 29 24.5	−24 30 54.8	0.96	1.03	...	...	1.0	17.67	0.87	...	F6–G9	G2.5	
4.....	36			16 29 27.7	−24 24 39.0	0.99	0.96	...	...	−1.5	17.45	0.78	...	F6–G0	F8	

NOTES.—Units of right ascension are hours, minutes, and seconds, and units of declination are degrees, arcminutes, and arcseconds. Table 2 is also available in machine-readable form in the electronic edition of the *Astronomical Journal*.

[a] Hydra field and aperture number of observation.

[b] Source names from optical or infrared studies are (SR) Struve & Rudkjøbing (1949); (DoAr) Dolidze & Arakelyan (1959); (GSS, Source 1) Grasdalen et al. (1973); (VSSG) Vrba et al. (1975); (VSS) Vrba et al. (1976); (EL) Elias (1978); (Chini) Chini (1981); (WL) Wilking & Lada (1983); (ROX) Montmerle et al. (1983); (WSB) Wilking et al. (1987); (WLY) Wilking et al. (1989); and (GY) Greene & Young (1992).

[c] X-ray source association from the *Einstein* survey by (ROX) Montemerle et al. (1983); the *ROSAT* survey by (ROXR1) Casanova et al. (1995) or (ROXRA, ROXRF) Grosso et al. (2000); the *Chandra* survey by (ROXCH) Imanishi et al. (2001), (GDS) Gagné et al. (2004), or (ROXC) N. Grosso et al. (2005, in preparation); or observations with *XMM-Newton* by (ROXN) Ozawa et al. (2005).

[d] CaH index calculated from the ratio of flux from the center of the continuum at 7035 Å to the center of the CaH absorption at 6975 Å.

[e] TiO index calculated from the ratio of flux from the center of the continuum at 7035 Å to the center of the TiO band at 7140 Å.

[f] Previously reported equivalent width of Hα by Cohen & Kuhi (1979), Bouvier & Appenzeller (1992), or Martín et al. (1998).

[g] References for spectral types are (CK) Cohen & Kuhi (1979); (BA) Bouvier & Appenzeller (1992); (GM) Greene & Meyer (1995); (MMGC) Martín et al. (1998); (LR) Luhman & Rieke (1999); (WGM) WGM99; and (N02) Natta et al. (2002).

[h] *R*- and *I*-band photometry from S. Gordon & K. Strom (1990, unpublished).

[i] Radio continuum source at $\lambda = 6$ cm observed by André et al. (1987), Leous et al. (1991), or Gagné et al. (2004).

[j] "Ca em" and "db Ca em" refer to Ca emission and double Ca emission, respectively.

[k] S/N in 6700 Å region is too low to detect Li absorption.

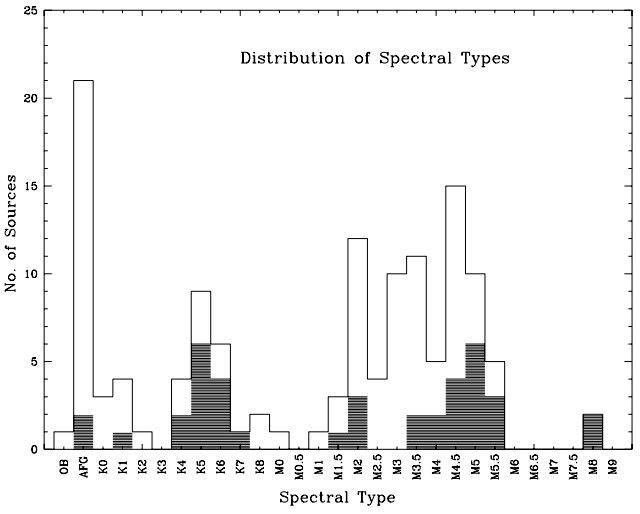

FIG. 4.—Distribution of spectral types derived for 131 program objects. The bins were chosen to permit a direct comparison with similar histograms derived for other star-forming regions (e.g., Hillenbrand 1997). The shaded areas indicate objects that displayed strong Hα emission [EW(Hα) > 10 Å].

Emission lines from both permitted and forbidden atomic transitions were detected in the spectra of the strongest Hα emitters in Table 3 with EW(Hα) > 28 Å. Both Pa 14 and O I (7773 Å) displayed broad profiles with FWHMs similar to that of Hα. The other O I lines and the He I lines all appeared to be barely resolved, with FWHMs between 150 and 180 km s^{-1}. The detection of forbidden-line emission from [O I] was observed in six objects. Weak [S II] emission at 6731 Å was detected in only two objects (SR 22 and WSB 46). The detection of these lines is consistent with the presence of winds associated with CTTSs (Edwards et al. 1987).

4.3. *Identification of Pre-Main-Sequence Association Members*

Pre-main-sequence objects that are products of recent star formation in the Ophiuchus region were identified using one or more of the following four criteria. First, candidates with Hα emission with EW > 10 Å resemble CTTSs, a property exhibited by 39 stars in our study (see Table 2, col. [11]). Second, association with X-ray emission is a signpost of youth and has been observed in 61 stars from our sample by various surveys of the region (see Table 2, col. [4]). Third, the presence of lithium absorption is an indicator of youth. While the lithium absorption was not well resolved in our spectra, it was definitely detected in 30 stars (Table 2, col. [9]). Finally, 58 objects (excluding giants identified in Table 2) that are too luminous to be main-sequence objects at the distance to ρ Oph *and* have an estimate for A_v too high to be foreground to the cloud (A_v > 1.5 mag) are identified as pre-main-sequence objects. Table 4 lists the 88 association members identified by our observations followed by the criteria used in their classification. At least 25 of these objects are newly identified association members. The bright association member SR 12 has been included in the list; while we did not obtain a spectrum, it was present in our *R*- and *I*-band images and had a previously well-determined spectral type.

We note that of the 26 objects with dwarflike surface gravities (Table 2), 19 are identified as association members based on the second, third, or fourth criterion. None display strong Hα emission. Without performing a quantitative analysis, the strengths of their CaH and Na I absorption lines are indistinguishable from those of main-sequence stars.

4.3.1. *Lithium*

The presence of Li I absorption at 6707 Å in stellar spectra indicates that the objects have cool interiors ($<2\times10^6$ K) and are young. Measurements proved to be difficult for most objects due to our spectral resolution and neighboring iron lines. The line was definitely observed in 30 stars with higher S/N spectra ("yes" in Table 2, col. [9]) and tentatively detected in 19 stars ("yes:" in Table 2, col. [9]). Four stars were identified as young objects solely on the basis of lithium absorption (Table 4), and all were located above the main sequence in the H-R diagram. The absence of a Li entry in Tables 2 and 4 does not imply that Li I is not present, only that the feature was not discernible in our spectra.

4.3.2. *Brown Dwarfs*

This program included seven brown dwarf candidates identified through low-resolution infrared spectroscopy: GY 3, GY 5, GY 37, GY 59, GY 204, GY 310, and GY 326 (WGM99; Luhman & Rieke 1999; Natta et al. 2002). The new optical spectral types agreed with the infrared classifications within two subclasses for six out of seven sources. Using infrared spectra, GY 310 was classified as M8.5 by WGM99 and B. A. Wilking et al. (2005, in preparation) and as M6 by Natta et al. (2002). While the spectrum is noisy, our optical classification of M4 for GY 310 is significantly earlier and, if confirmed, may suggest the presence of an infrared companion.

The two coolest objects in our sample, 4-41 (GY 3) and 4-45 (GY 264), are classified with M8 spectral types. Their spectra, shown in Figure 1*d*, feature strong VO absorption at 7334–7534 and 7851–7973 Å. The shorter wavelength VO forms a obvious depression in the continuum between two TiO bands. The longer wavelength VO broadens the absorption from the 7666–7861 TiO band starting around 7900 Å. Their classification as young brown dwarf candidates was confirmed by their strong Hα emission [EW(Hα) = 140 and 155 Å, respectively], association with X-ray emission (see Table 2), and location in the H-R diagram (§ 4.4). Object 4-41, also known as ISO Oph 32, was first identified as a low-mass object by Natta et al. (2002). Excess emission at *K* ($r_k = 0.34$) and in the mid-infrared (Bontemps et al. 2001) are indicative of a circumstellar disk (Natta et al. 2002).[3] Object 4-45 is a previously unidentified brown dwarf candidate. It was previously misidentified as a foreground M star based on *VRI* photometry (ophmd5; Festin 1998). It does not appear to have an infrared excess with $r_k = 0.02$. The object lies in close proximity to the marginal Herbig-Haro candidate P2 (Phelps & Barsony 2004).

4.3.3. *Distribution of Association Members*

The distribution of the 88 association members identified by this study is shown in Figure 6 relative to contours of ^{13}CO column density that delineate the cloud boundaries. We note that due to the high extinction in the cloud core, our data sample only the surface population toward the densest gas. For reference, star symbols mark the locations of the Sco-Cen B star ρ Oph A and the most massive member of the L1688 embedded cluster, Oph S1. There is a definite tendency for association members to concentrate near the highest column density gas in

[3] Using *JHK* photometry from the 2MASS catalog converted into the California Institute of Technology photometric system, $r_k = F_{K,\mathrm{ex}}/F_K = [(1+r_h)(10^{[(H-K)-(H-K)_0-0.065A_v]/2.5})]-1$, where $r_h = F_{H,\mathrm{ex}}/F_H = (10^{[(J-H)-(J-H)_0-0.11A_v]/2.5})-1$, with intrinsic colors and visual extinctions computed for an M8 spectral type.

TABLE 3

GAUSSIAN FITS TO EMISSION LINES OF T TAURI STARS

			He I λ5876[c]		[O I] λ6300[c,d]		Hα λ6563[c,e]			He I λ6678[c]		He I λ7066[c]		O I λ7773[c]		O I λ8447[c]		Ca II λ8498[c]		Ca II λ8542[c]		Pa 14 λ8598[c]		Ca II λ8662[c]	
FIELD[a]	APERTURE[a]	NAME(S)[b]	W_λ (Å)	Δv (km s^{-1})	W_λ (Å)	Δv (km s^{-1})	W_λ (Å)	Δv (km s^{-1})	Type	W_λ (Å)	Δv (km s^{-1})	W_λ (Å)	Δv (km s^{-1})	W_λ (Å)	Δv (km s^{-1})	W_λ (Å)	Δv (km s^{-1})	W_λ (Å)	Δv (km s^{-1})	W_λ (Å)	Δv (km s^{-1})	W_λ (Å)	Δv (km s^{-1})	W_λ (Å)	Δv (km s^{-1})
2	10	...	...	...	...	...	14	180	I	...	...	...	...	...	...	...	...	...	...	...	...	...	...	...	...
1	7	SR 22	...	...	3.0:	95	35	220	I	...	...	...	...	...	...	...	...	...	...	...	...	...	...	...	...
3	15	IRS 3	...	...	...	...	34	260	I	0.64:	135	...	...	...	...	...	...	...	...	...	...	...	...	...	...
2	25	...	...	...	...	...	13	300	IIR	...	...	...	...	...	...	...	...	...	...	...	...	...	...	...	...
3	18	Same as 2-25	...	...	...	...	16	360	IIR	...	...	...	...	...	...	...	...	...	...	...	...	...	...	...	...
1	29	SR 4	3.3	300	...	...	70	320	I	0.73:	480	0.37:	130	1.4	290	2.8	290	10	220	11	230	1.4:	260:	9.6	230
2	1	Chini 8	...	...	...	...	9.6	160	I	...	...	...	...	...	...	...	...	...	...	...	...	...	...	...	...
3	24	Same as 2-1	...	...	...	...	>13	170	IIB	...	...	...	...	...	...	...	...	...	...	...	...	...	...	...	...
2	19	...	...	...	...	...	13	160	I	...	...	...	...	...	...	...	...	...	...	...	...	...	...	...	...
1	5	GSS 28	...	...	...	...	27	240	I	...	...	...	...	...	...	...	...	...	...	...	...	...	...	...	...
1	25	WSB 28	...	...	...	...	11	290	I	...	...	...	...	...	...	...	...	...	...	...	...	...	...	...	...
4	16	GY 5	...	...	...	...	20	190	I	...	...	...	...	...	...	...	...	...	...	...	...	...	...	...	...
4	41	GY 3	20:	230	...	...	>160	210	Iw	4.1	170	0.69:	80	...	...	...	...	0.71:	150	1.0	120	...	...	0.82	190
1	28	DoAr 25	...	...	...	...	12	250	I	...	...	...	...	...	...	...	...	...	...	...	...	...	...	...	...
2	27	EL 24	2.8:	240	...	...	>48	240	Iw	0.75:	160	0.36:	100	0.28:	140	1.6	240	4.5	180	5.0	160	...	...	4.4	150
3	25	Same as 2-27	1.7U	200	...	...	>53	280	IIIB	0.39U	150	0.33:	110	0.91	260	2.0	220	7.7	200	8.1	190	...	...	7.3	180
4	66	GY 37	...	...	...	...	9.9	210	I	...	...	...	...	...	...	...	...	...	...	...	...	...	...	...	...
2	36	WSB 34	5.7	180	...	...	56	240	I	1.9	170	0.75	150	1.4	310	...	...	...	...	...	...	...	...	...	...
4	4	...	...	...	...	...	15	150	I	...	...	...	...	...	...	...	...	...	...	...	...	...	...	...	...
2	29	WSB 37	1.4U	170	...	...	23	250	I	0.44U	160	0.30U	150	...	...	...	...	...	...	...	...	...	...	...	...
3	3	Same as 2-29	4.0:	160	...	...	28	270	I	1.1:	150	0.52:	140	...	...	...	...	...	...	...	...	...	...	...	...
1	36	WSB 38	...	...	...	...	12	260	I	...	...	...	...	...	...	...	...	...	...	...	...	...	...	...	...
1	32	WSB 40	...	...	...	...	>27	210	IIIB	...	...	...	...	1.4:	330:	3.5	150	12.8	140	13.5	160	...	...	12	140
4	53	WL 18	...	...	...	...	130	260	IIIB	2.7:	130	...	...	...	...	3.2	140	28	180	33	200	3.9[f]	230	24	190
4	46	...	...	...	...	...	17	310	I	...	...	...	...	...	...	...	...	...	...	...	...	...	...	...	...
1	37	SR 24s	...	...	3.0	230	>52	470	IIB	...	...	...	...	0.87:	220	3.8	320	8.3	260	8.4	240	1.0U	240U	7.3	220

TABLE 3—*Continued*

			He I λ5876[c]		[O I] λ6300[c,d]		Hα λ6563[c,e]			He I λ6678[c]		He I λ7066[c]		O I λ7773[c]		O I λ8447[c]		Ca II λ8498[c]		Ca II λ8542[c]		Pa 14 λ8598[c]		Ca II λ8662[c]	
Field[a]	Aperture[a]	Name(s)[b]	W_λ (Å)	Δv (km s^{-1})	W_λ (Å)	Δv (km s^{-1})	W_λ (Å)	Δv (km s^{-1})	Type	W_λ (Å)	Δv (km s^{-1})	W_λ (Å)	Δv (km s^{-1})	W_λ (Å)	Δv (km s^{-1})	W_λ (Å)	Δv (km s^{-1})	W_λ (Å)	Δv (km s^{-1})	W_λ (Å)	Δv (km s^{-1})	W_λ (Å)	Δv (km s^{-1})	W_λ (Å)	Δv (km s^{-1})
4.....	65	GY 204	2.8:	170	6.2	280	42	260	I	2.2:	220	0.54U	110	...	...	...	...	4.1	600	3.2	480	...	...	1.8	290
4.....	10	...	11	160	2.9	100	100	230	Iw	3.4	120	1.4	100	2.2	220	2.9	140	2.6	140	3.1	130	...	...	2.5	130
1.....	6	WSB 48	...	...	...	...	120	260	I	...	...	...	...	...	...	...	...	...	...	...	...	...	...	...	...
3.....	6	WSB 49	1.9:	140	...	...	40	200	I	0.58:	120	0.36U	170	...	...	0.84:	130	...	...	...	...	...	...	...	...
4.....	45	GY 264	24	160	...	...	>210	200	Iw	5.9	140	1.9	120	...	...	...	...	1.2:	150	1.3	120	...	...	0.65	90
2.....	35	WSB 51	...	...	...	...	13	240	I	...	...	...	...	...	...	...	...	...	...	...	...	...	...	...	...
4.....	24	IRS 49	...	...	...	...	20	230	I	...	...	...	...	...	...	...	...	...	...	...	...	...	...	...	...
1.....	31	WSB 53	...	...	...	...	20	210	IIIB	...	...	...	...	...	...	...	...	...	...	...	...	...	...	...	...
3.....	5	WSB 52	...	...	...	...	42	310	I	...	...	...	...	0.52	270	1.7	220	1.5	150	1.8	120	...	...	1.5	150
1.....	26	SR 9	...	...	...	...	24	260	I	...	...	...	...	...	...	...	...	...	...	...	...	...	...	...	...
1.....	24	SR 10	2.9	160	...	...	62	310	I	1.4	150	0.26U	90	1.0:	280	2.0	210	12	160	13	170	...	...	9.7	140
3.....	31	...	...	...	...	...	14	160	I	...	...	...	...	...	...	...	...	...	...	...	...	...	...	...	...
3.....	20	WSB 60	7.8	160	3.0	95	95	230	I	1.3	120	0.54	100	...	...	...	...	3.5	140	3.8	140	...	...	2.6	130
2.....	30	...	...	...	...	...	40	320	I	...	...	...	...	...	...	...	...	...	...	...	...	...	...	...	...
3.....	42	Same as 2-30	...	...	...	...	>10	420	IIR	...	...	...	...	...	...	...	...	...	...	...	...	...	...	...	...
1.....	35	SR 20	...	...	...	...	>16	270	IIIB	...	...	...	...	...	...	...	...	10	[g]	8.6	[g]	...	...	7.0	[g]
2.....	31	Same as 1-35	...	...	...	...	>15	260	IIIB	...	...	...	...	...	...	...	...	10	[g]	8.7	[g]	...	...	7.8	[g]
1.....	15	SR 13	3.7	150	2.6	160	>50	200	Iw	1.4	110	0.60:	100	...	...	0.48U	160	0.6	110	0.81:	100	...	...	0.46U	90
3.....	43	WSB 63	...	...	...	...	60	320	I	...	...	0.23:	160	...	...	0.49	150	...	...	...	...	...	...	...	...

NOTE.—Table 3 is also available in machine-readable form in the electronic edition of the *Astronomical Journal*.

[a] Hydra field and aperture number of observation.

[b] Source names as noted in Table 2.

[c] Equivalent widths in angstroms and the FWHM in kilometers per second of the emission line as determined from Gaussian fits. The fit parameters are greater than 5 σ unless otherwise noted. Values followed by a colon are between 3 and 5 σ, and values followed by a "U" are upper limits. The values for FWHM have not been deconvolved by the instrumental response.

[d] The [O I] line at 6363 Å is also observed in emission but is much weaker.

[e] The profile shape of Hα as defined by Reipurth et al. (1996): symmetric (type I), double-peaked with the secondary peak greater than half the strength of the primary (type II), or double-peaked with the secondary peak less than half the strength of the primary (type III). The Roman numeral is followed by "B" if the asymmetry is on the blue side, "R" if it is on the red side, or "w" if the profile has non-Gaussian wings. Multiple Gaussian fits were used to estimate the equivalent width for type II or III profiles. Equivalent widths for profiles with wings are lower limits. Velocity widths for type II or III profiles are not well defined.

[f] Pa 19 at 8413 Å was also detected in the spectrum of WL 18 with $W\lambda = 1.9$: Å and $\Delta v = 180$: km s^{-1}.

[g] The Ca II emission lines display double-peaked type IIIB profiles similar to Hα.

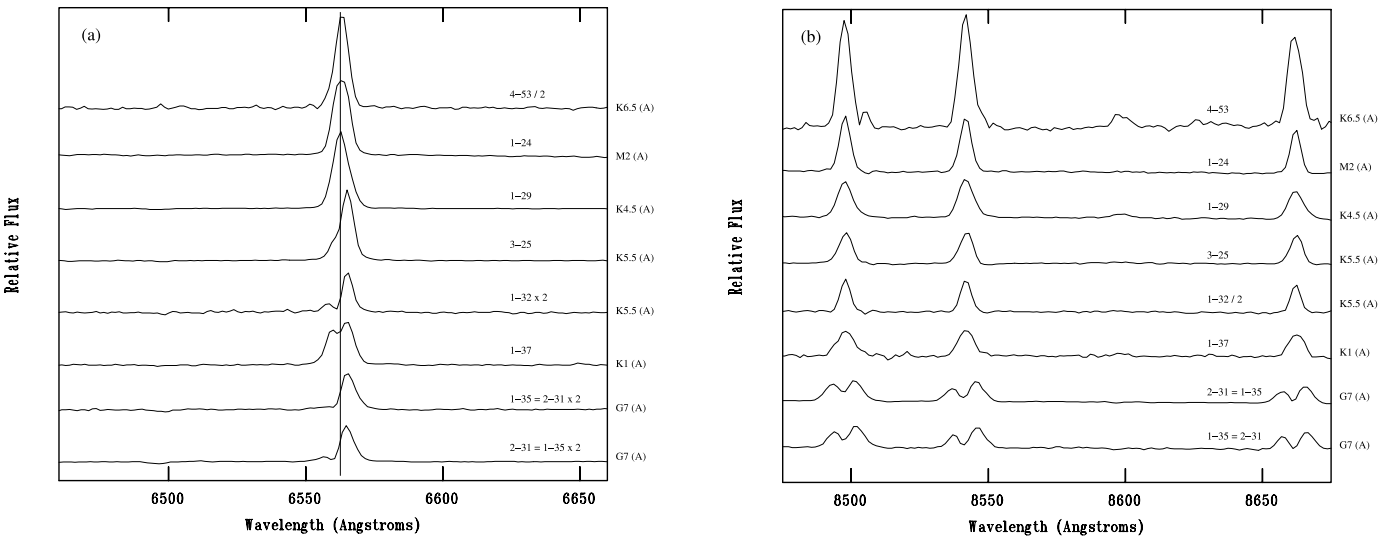

FIG. 5.—Expanded view of Hα and Ca II emission lines in seven CTTSs labeled with their field and aperture numbers (Table 2) and spectral types. The bottom two spectra in each panel are from the same source observed on two different nights. (*a*) Structure of the Hα emission line, with the rest wavelength of Hα marked as a reference. (*b*) Ca II triplet for the same objects.

the core. Only 14 members are seen in projection outside the lowest contour, corresponding to $N_{\rm LTE}(13) = 6 \times 10^{14}$ cm^{-2}.

4.4. *Hertzsprung-Russell Diagram*

With the benefit of the spectroscopic data, we can investigate the ages and masses of the association members identified by this study. The intrinsic colors, bolometric corrections, and temperature scale for dwarf stars were derived from the works of Schmidt-Kaler (1982) for B8–K5 stars and from Bessell (1991) for K5–M7 stars. We note that the assumption of dwarf, rather than subgiant, surface gravities will overestimate $T_{\rm eff}$ for stars with spectral types of G5–K5 by <250 K and underestimate $T_{\rm eff}$ for stars with spectral types of M2–M8 by <200 K. For the B3 star Source 1, an effective temperature of $T_{\rm eff} = 19{,}000$ and an $L_* = 1500\,L_\odot$ was adopted (e.g., Lada & Wilking 1984). For the M8 brown dwarf candidates, we assumed values of $T_{\rm eff} = 2500$, $(R-I)_0 = 2.5$, and BC$(I) = -1.7$ that are consistent with recent studies of very low mass stars (Dahn et al. 2002; Hawley et al. 2002). Bolometric luminosities were computed from the *I*-band magnitudes in the following way. Magnitudes were dereddened using the $(R-I)$ color excess derived from the observed minus intrinsic $(R-I)$ color for the corresponding spectral type and using the reddening law $A_v/E(R-I) = 6.25$ (Cohen et al. 1981). In a few cases the errors in the photometry and/or spectral classification yielded slightly negative values for the extinction, and an extinction of 0.0 was assumed. Absolute *I* magnitudes were then computed, assuming a distance of 150 pc (de Zeeuw et al. 1999), and converted to bolometric magnitudes using the appropriate bolometric correction for the observed spectral type. The stellar luminosity was computed using $\log(L/L_\odot) = 1.89 - 0.4M_{\rm bol}$, assuming $M_{\rm bol,\odot} = 4.74$ (Livingston 1999). Due to the dominance of emission lines in the spectrum of WL 18, we adopted the luminosity estimated by Bontemps et al. (2001) from the *J*-band flux and $(J-H)$ color, adjusted to a distance of 150 pc.

The resulting H-R diagram is presented in Figure 7 for 84 association members relative to the theoretical tracks and isochrones of D'Antona & Mazzitelli (1997) and F. D'Antona & I. Mazzitelli (1998, private communication). Excluded from the diagram is the B3 star Source 1, the A7 star VSSG 14, and objects GY 59 and GY 326, which lack *R*-band photometry and therefore estimates for A_v and $\log L$. CTTSs are indicated by filled diamonds; open diamonds represent association members with weak or no Hα emission that would correspond to WTTSs or post–T Tauri stars. The errors in $T_{\rm eff}$ are estimated to be ± 105 K for K–M stars with equal contributions from the uncertainties in the spectral classification and systematic offsets in the temperature scale. The uncertainty in $\log L$ is estimated to be 0.12 dex, assuming uncertainties in the *R* and *I* photometry of 0.04 mag, in the distance modulus of 0.15 mag, and in the bolometric correction of 0.1 mag. The masses and ages interpolated from the models are given in Table 4 with uncertainties due to random errors of 20% in mass and 0.25 dex in log (age). Comparisons with the Baraffe et al. (1998) models suggest systematic errors between different sets of models of $\sim$50% in mass and $\sim$0.5 dex in log (age) (e.g., Hillenbrand & White 2004).

The median age of the association members in Figure 7 is 2.1 Myr. There is no significant difference observed in the median age of the CTTS and non-CTTS association members. Following the analysis of Preibisch & Zinnecker (1999), the apparent age spread observed in Figure 7 is consistent with all the association members having roughly the same age (1–3 Myr) with the scatter in the age accounted for by the errors noted above and unresolved binaries.

5. IMPLICATIONS FOR THE STAR FORMATION HISTORY

The association members identified in this study are pre-main-sequence objects distributed over a 1.3 deg^2 area (6.8 pc^2) and lie within a projected radius of 2 pc of the highest extinction regions of the main ρ Oph cloud (see Fig. 6). The fact that our derived visual extinctions are generally low (80% of the association members have $A_v \leq 5$ mag) indicates that the majority of our sample lies at the surface of the cloud. Recent spectroscopic studies of YSOs in the ρ Oph cloud have focused on the embedded population in the 1 pc $\times$ 2 pc centrally condensed core and have necessarily been conducted at near-infrared wavelengths (Greene & Meyer 1995; Luhman & Rieke 1999; WGM99; Natta et al. 2002). These studies have consistently derived ages between 0.1 and 1 Myr when using the D'Antona & Mazzitelli (1997) tracks and isochrones, with a median age of 0.3 Myr. After considering our uncertainties, we conclude that the distributed

TABLE 4

ASSOCIATION MEMBERS

Field	Aperture	Name	A_v (mag)	$M(I)$ (mag)	log $T_{\rm eff}$ (K)	log $(L/L_\odot)$	M_*[a] $(M_\odot)$	log (age)[a] (Myr)	Notes[b]
2	15		2.6	6.26	3.512	−0.76	0.19	6.09	li, ext
2	14		2.1	8.03	3.525	−1.50	0.27	7.28	ext
2	10		0.8	8.13	3.477	−1.38	0.14	6.57	ha
1	7	SR 22	0.0	7.00	3.488	−0.98	0.15	6.18	ha, x
3	15	WLY 2-3	4.9	6.04	3.544	−0.74	0.31	6.33	ha, x, ext
2	32		2.6	6.79	3.512	−0.98	0.20	6.32	x, li, ext
1	22	VSS 23	5.1	3.43	3.630	0.25	0.53	5.59	x, ext
2	25	WLY 2-11	2.3	7.25	3.477	−1.03	0.14	6.17	ha, ext, x
1	29	SR 4	0.5	5.15	3.650	−0.43	0.91	7.01	ha, x, li
1	38	GSS 20	6.0	3.54	3.630	0.21	0.54	5.64	x, ext
3	14		1.0	7.36	3.488	−1.12	0.16	6.33	li
2	1	Chini 8	0.0	7.12	3.462	−0.93	0.12	5.57	ha, x, li
4	28		5.3	5.93	3.525	−0.66	0.22	6.06	x, ext
1	13	VSSG 19	3.4	5.05	3.544	−0.35	0.27	5.83	x, ext
2	19		2.1	6.63	3.488	−0.83	0.15	6.01	ha, li, ext
1	5	GSS 28	2.8	4.28	3.650	−0.08	0.79	6.31	ha, x, li, ext
4	39		1.9	6.06	3.512	−0.68	0.18	6.01	li, ext
2	11		0.1	7.39	3.482	−1.11	0.15	6.30	x, li
1	25	WSB 28	2.9	5.48	3.544	−0.52	0.29	6.02	ha, x, ext
4	16	GY 5	2.8	8.27	3.462	−1.39	0.11	6.47	ha, x, ext
4	41	GY 3	0.0.	9.74	3.398	−1.33	<0.04	<5.0	ha, x
1	30	GSS 31	6.0	2.26	3.752	0.82	2.10	6.50	x, ext
1	28	DoAr 25	2.9	3.97	3.638	0.03	0.64	5.97	ha, x, li, ext
2	27	EL 24	7.5	3.57	3.630	0.19	0.54	5.66	ha, x, ext
4	18		2.2	8.64	3.488	−1.64	0.16	7.00	ext
4	25		1.3	9.12	3.462	−1.73	0.09	6.74	x
4	66	GY 37	3.4	9.95	3.477	−2.11	0.10	7.31	ha, x, ext
4	27	GY 59	...	...	3.491	...	...	...	x
2	36	WSB 34	0.8	7.80	3.488	−1.30	0.16	6.55	ha
1	2	Source 1	13	−1.15	4.278	3.20	5.00	7.60	x, ext
4	4		1.9	8.51	3.477	−1.53	0.14	6.74	ha, x, ext
2	29	WSB 37	0.8	7.00	3.477	−0.93	0.14	6.04	ha, x, li
1	21		4.3	4.83	3.591	−0.29	0.48	6.08	ext, x
3	22		0.4	7.74	3.488	−1.28	0.16	6.52	li, x
1	20	GY 112	2.4	5.92	3.525	−0.65	0.22	6.05	x, ext
4	13		4.6	6.87	3.525	−1.03	0.24	6.52	li, ext
1	36	WSB 38	7.7	1.87	3.765	0.98	2.20	6.45	ha, x, li, ext
4	30		2.8	7.62	3.488	−1.23	0.16	6.46	x, li, ext
1	32	WSB 40	5.6	3.68	3.630	0.15	0.55	5.71	ha, ext
4	53	WL 18	10.4[c]	6.89	3.612	−0.66[c]	0.78	7.10	ha, x, ext
2	38		1.7	7.89	3.488	−1.34	0.16	6.60	ext
4	46		8.8	5.16	3.602	−0.42	0.61	6.45	ha, ext, x
1	37	SR 24s	5.5	3.68	3.705	0.21	1.40	6.64	ha, x, ext
4	63		2.6	7.89	3.488	−1.33	0.16	6.59	ext
4	65	GY 204	0.5	9.25	3.462	−1.78	0.09	6.77	ha, x
4	37		6.7	6.27	3.535	−0.82	0.27	6.34	ext
3	44	WSB 45	0.0	7.43	3.488	−1.15	0.16	6.37	li, x
1	9	WSB 46	0.6	6.01	3.544	−0.73	0.31	6.31	x
3	17		8.6	4.00	3.705	0.08	1.30	6.81	ext
4	10		4.4	6.97	3.512	−1.04	0.20	6.40	ha, ext
1	6	WSB 48	0.0	7.35	3.491	−1.18	0.16	6.42	ha
...	...	SR 12	2.4	3.76	3.580	0.15	0.31	4.99	x, ext
3	6	WSB 49	0.3	7.24	3.493	−1.10	0.16	6.34	ha, x, li
4	45	GY 264	0.0	9.84	3.398	−1.37	<0.04	<5.0	ha, x
3	7		0.0	8.44	3.482	−1.53	0.15	6.80	x
2	20		1.1	7.75	3.544	−1.43	0.36	7.46	x
4	22	GY 284	4.8	7.45	3.519	−1.25	0.24	6.80	x, ext
2	6	WSB 50	1.9	7.04	3.488	−1.00	0.15	6.20	x, li, ext
4	54		3.0	6.05	3.535	−0.73	0.26	6.22	li, ext
2	35	WSB 51	4.3	3.85	3.621	0.08	0.51	5.74	ha, x, li, ext
4	24	WLY 2-49	9.6	3.88	3.630	0.07	0.57	5.82	ha, x, ext
1	31	WSB 53	3.7	3.94	3.630	0.04	0.58	5.87	ha, ext
3	5	WSB 52	7.1	3.90	3.638	0.06	0.63	5.92	ha, x, li, ext
1	26	SR 9	0.0	5.38	3.638	−0.53	0.85	7.10	ha, x, li
2	34		4.1	5.04	3.544	−0.34	0.27	5.82	x, ext
4	64	GY 326	...	...	3.544	...	...	...	x
3	21		0.4	7.99	3.488	−1.37	0.16	6.64	li

TABLE 4—*Continued*

Field	Aperture	Name	A_v (mag)	$M(I)$ (mag)	log $T_{\rm eff}$ (K)	log $(L/L_\odot)$	M_*[a] $(M_\odot)$	log (age)[a] (Myr)	Notes[b]
1	14	VSSG 14	6.7	2.24	3.895	0.94	1.70	7.15	x, ext
1	10	ROX 31	5.0	3.79	3.597	0.13	0.38	5.53	x, ext
1	24	SR 10	0.1	5.99	3.544	−0.73	0.31	6.31	ha, x
3	34	WSB 58	0.9	7.00	3.482	−0.95	0.14	6.11	x
3	31		0.9	7.11	3.477	−0.97	0.14	6.09	ha, x, li
2	3		3.0	6.21	3.525	−0.77	0.23	6.18	li, ext
2	21		3.5	6.27	3.491	−0.75	0.15	5.77	ext
3	11	ROX 32	3.5	5.69	3.525	−0.56	0.21	5.94	x, li, ext
3	20	WSB 60	2.0	7.38	3.488	−1.13	0.16	6.34	ha, ext
3	12		1.9	6.53	3.525	−0.90	0.24	6.34	ext
4	3		4.0	7.27	3.512	−1.17	0.21	6.59	ext
2	37		4.7	6.24	3.535	−0.81	0.27	6.32	ext, x
2	30		6.8	4.62	3.638	−0.22	0.76	6.44	ha, ext, x
2	4		4.8	5.87	3.544	−0.68	0.30	6.24	ext, x
3	39		0.5	8.61	3.477	−1.57	0.14	6.79	li
4	57		5.3	6.88	3.512	−1.01	0.20	6.36	ext
1	35	SR 20	5.7	2.08	3.747	0.89	2.20	6.41	ha, x, ext
2	23		1.4	7.73	3.482	−1.25	0.15	6.45	li, x
1	15	SR 13	0.0	5.07	3.491	−0.27	0.13	4.55	ha, x
3	43	WSB 63	3.8	5.37	3.553	−0.48	0.34	6.04	ha, li, ext, x
3	37		0.0	8.61	3.462	−1.52	0.10	6.57	li

NOTE.—Table 4 is also available in machine-readable form in the electronic edition of the *Astronomical Journal*.

[a] Masses and ages derived relative to the theoretical tracks and isochrones of D'Antona & Mazzitelli (1997) and F. D'Antona & I. Mazzitelli (1998, private communication).

[b] Association membership established through the presence of Hα emission (ha), X-ray emission (x), lithium absorption (li), or location above the main sequence and $A_v > 1.5$ mag (ext).

[c] Due to strong emission lines in the R and I bands relative to the continuum, the A_v and luminosity estimates are taken from Bontemps et al. (2001) using the $(J - H)$ color and adjusted to a distance of 150 pc.

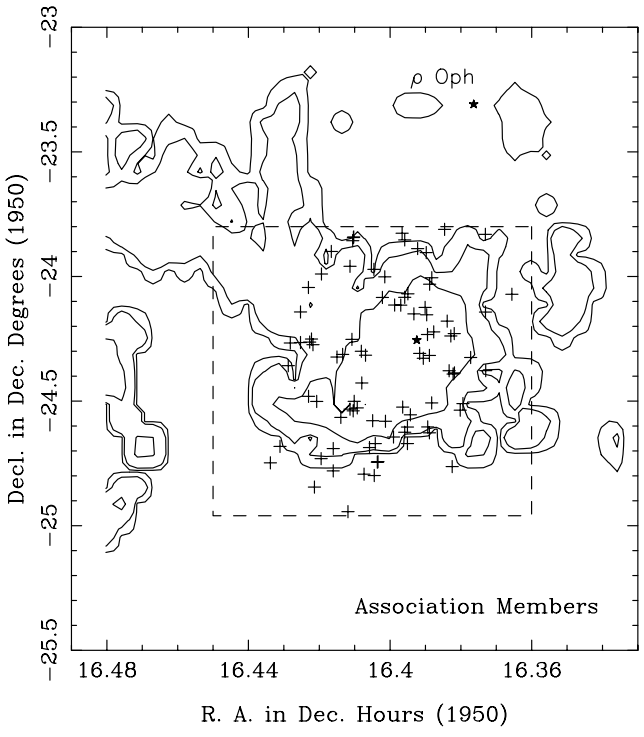

FIG. 6.—Distribution of association members relative to contours of ^{13}CO column density. The contours were computed from Loren (1989) assuming LTE and $T_{\rm ex} = 25$ K. The values of the contours in units of cm^{-2} are 6×10^{14}, 3×10^{15}, and 1.5×10^{16}; the lowest contour delineates the outer boundary of the dark cloud. The dashed box outlines the field included in our Hydra observations. Star symbols mark the locations of the star ρ Oph A (labeled) and the embedded association member Oph S1 in the L1688 core.

population is significantly older than that in the more highly extincted cloud core.

The question then arises as to the origin of this more distributed population. One explanation is that these objects formed in the dense core and have diffused or been ejected to the surface of the cloud. However, the space motion of a YSO that acquires the velocity dispersion of the molecular gas in which it formed (1–2 km s^{-1}) would not be high enough to move an object to the projected distances from the core of >1 pc that we observe for some association members. Alternatively, the ejection of very low mass stars and brown dwarfs from small groups has been proposed for the origin of widely distributed WTTSs and of substellar objects (Sterzik & Durisen 1995; Reipurth & Clarke 2001; Bate et al. 2002). In this case, one would predict that the lowest mass association members in our sample would display a higher velocity dispersion (and thus a broader spatial distribution) than YSOs in the core. We have analyzed the distribution of the higher mass association members ($M > 0.5\ M_\odot$) relative to the lower mass members ($M < 0.5\ M_\odot$) using a two-dimensional Kolmogorov-Smirnov (K-S) test. The K-S statistic is consistent with the two populations being drawn from the same parent population. Our data do not lend support to the ejection hypothesis; however, our sample includes only eight brown dwarf candidates.[4]

A second possibility is that the association members at the cloud edges are near their birth sites and that the dense gas in L1688 was once distributed over a larger area than we see today. It has been proposed that star formation in Upper Sco was triggered about 5 Myr ago by the passage of an expanding H I

[4] Radial velocity measurements are required for a detailed analysis of the kinematics of these stars to reject the hypothesis that they were ejected from the cloud as the result of the dissolution of small stellar groups.

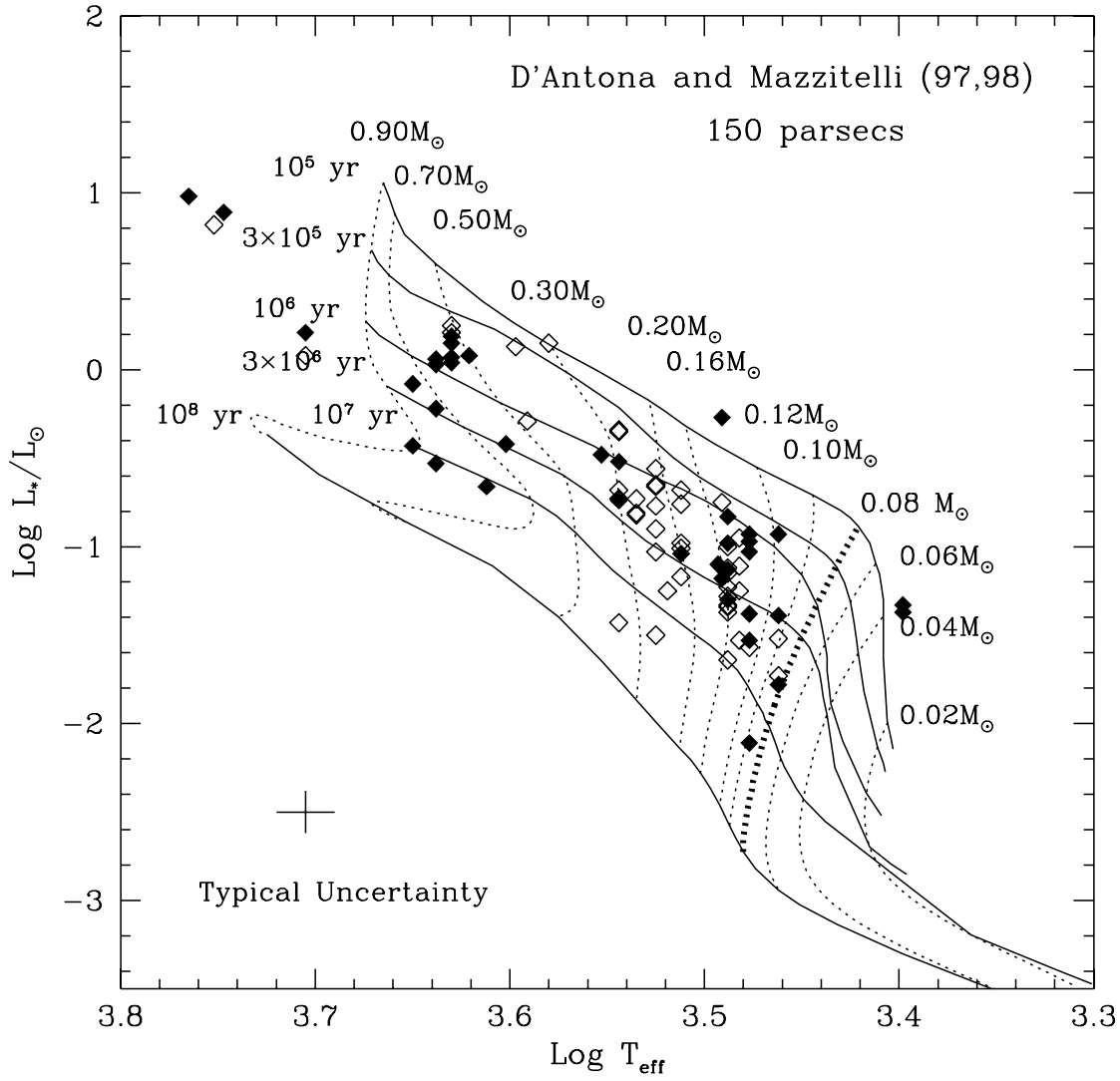

FIG. 7.—H-R diagram for the ρ Oph association members with optically determined spectral types. The filled diamonds indicate the positions of CTTSs [EW(Hα) $>$ 10 Å], and the open diamonds correspond to WTTSs or post–T Tauri stars relative to the theoretical tracks of D'Antona & Mazzitelli (1997) and F. D'Antona & I. Mazzitelli (1998, private communication). Isochrones shown as solid lines are 10^5, 3×10^5, 10^6, 3×10^6, 10^7, and 10^8 yr. Evolutionary tracks from 0.02 to 0.90 $M_\odot$ are shown by dashed lines. The bold dashed line marks the evolutionary track for a star at the hydrogen-burning limit. The typical error bar for a candidate is shown at the bottom left and is ±0.015 dex in $\log T_{\rm eff}$ and ±0.12 dex in $\log(L_{\rm bol}/L_\odot)$.

shell driven by massive stars in the Upper Centaurus–Lupus association (de Geus 1992). This age is consistent with that of high-mass stars in Upper Sco derived from a color-magnitude diagram and from the main-sequence turnoff (Preibisch et al. 2002; see models by Bertelli et al. 1994). The implied age of the low-mass stars in Upper Sco is also 5 Myr, but only after corrections are made for unresolved binaries (Preibisch & Zinnecker 1999). A comparison of Figure 7 with H-R diagrams for low-mass members of the Upper Scorpius subgroup, using the same set of theoretical evolutionary tracks and isochrones and not corrected for unresolved binaries, shows no discernible difference in age or age spread (e.g., Preibisch & Zinnecker 1999; Preibisch et al. 2001, 2002). This is not too surprising given that the ρ Oph cloud is ringed by high-mass members of Upper Sco such as the multiple star ρ Oph and σ Sco to the west and 22 Sco, α Sco, and τ Sco to the east. Therefore, one could regard the distributed population we observe as either low-mass members of the Upper Scorpius subgroup or older members of the ρ Oph cloud whose formation was contemporaneous with stars in the Upper Scorpius subgroup. In either scenario, ultraviolet radiation and the passage of an expanding shell from massive stars in the Upper Scorpius subgroup within the last 2.5 Myr would have stripped away the outer skin of the ρ Oph cloud, revealing the present population and perhaps triggering a second episode of star formation in the centrally condensed core (de Geus 1992).

6. SUMMARY

We have analyzed optical spectra for 139 candidate CTTSs that extend over a 1.3 deg^2 area in the direction of the main ρ Oph cloud. Of the 131 stars for which spectral types and surface gravities are estimated, 6 are identified as giants and 79 are classified as M stars. Association with the cloud is established for 88 objects by the presence of optical emission lines or lithium absorption in the spectra, by location in the H-R diagram, and/or by previously reported X-ray emission. Thirty-nine of the stars display strong Hα emission (EW $>$ 10 Å) characteristic of CTTSs. These emission lines are broad (FWHM $\sim$ 250 km s^{-1}), consistent with their origin in magnetospheric accretion columns. In addition, asymmetries in the Hα profiles and the presence of

forbidden lines observed in 16 objects are a signpost of mass outflows. A subset of the CTTSs also displays emission from the Ca II triplet that is strongest in the most massive CTTSs and, in one instance, self-absorbed. Two of the strongest emission-line objects are young, X-ray-emitting brown dwarf candidates with M8 spectral types.

Association members are distributed in the lower extinction regions surrounding the high-extinction core. An H-R diagram suggests a median age of 2.1 Myr with an apparent age spread due mainly to uncertainties in the calculated luminosity and the presence of unresolved binaries. This age is significantly older than the median age of 0.3 Myr for objects in the high-extinction core. There is no difference in median age between the CTTS and non-CTTS association members, and there are no statistically significant correlations between the age or mass of an association member and its projected distance from the core center. The age and distribution of this population is indistinguishable from that of low-mass stars in the Upper Scorpius subgroup. We propose that these stars formed in what was once a larger ρ Oph cloud. In this instance, star formation in the outer regions of the ρ Oph cloud would have been triggered by the same event that initiated star formation in Upper Sco.

We thank Di Harmer for obtaining the Hydra data through the WIYN Queue Observing Program and for assistance with the data reduction. Lori Allen provided helpful insight into the spectral-typing process and made available the bulk of the spectral standards used in this study in digital form. We gratefully acknowledge Eric Mamajek for helpful discussions. M. R. M. acknowledges support for this work through a Cottrell Scholar's Award from the Research Corporation. B. W. and J. R. acknowledge support from NSF AST 98-20898 to the University of Missouri—St. Louis and from the Missouri Research Board.

REFERENCES

Alcalá, J. M., Covino, E., Torres, G., Sterzik, M. F., Pfeiffer, M. J., & Neuhäuser, R. 2000, A&A, 353, 186
Alcalá, J. M., et al. 1996, A&AS, 119, 7
Allen, L. E. 1995, Ph.D. thesis, Univ. Massachusetts
Allen, L. E., & Strom, K. M. 1995, AJ, 109, 1379
André, P., & Montmerle, T. 1994, ApJ, 420, 837
André, P., Montmerle, T., & Feigelson, E. D. 1987, AJ, 93, 1182
Baraffe, I., Charbrier, G., Allard, F., & Hauschuldt, P. H. 1998, A&A, 337, 403
Bate, M. R., Bonnell, I. A., & Bromm, V. 2002, MNRAS, 332, L65
Bertelli, G., Bressan, A., Chiosi, C., Fagotto, F., & Nasi, E. 1994, A&AS, 106, 275
Bessell, M. S. 1991, AJ, 101, 662
Blaauw, A. 1991, in The Physics of Star Formation and Early Stellar Evolution, ed. C. J. Lada & N. D. Kylafis (NATO ASI Ser. C, 342; Dordrecht: Kluwer), 125
Bontemps, S., et al. 2001, A&A, 372, 173
Bouvier, J., & Appenzeller, I. 1992, A&AS, 92, 481
Casanova, S., Montmerle, T., Feigelson, E. D., & André, P. 1995, ApJ, 439, 752
Chini, R. 1981, A&A, 99, 346
Cohen, J. G., Frogel, J. A., Persson, S. E., & Elias, J. H. 1981, ApJ, 249, 481
Cohen, M., & Kuhi, L. V. 1979, ApJS, 41, 743
Cutri, R. M., et al. 2003, 2MASS All-Sky Catalog of Point Sources (Pasadena: IPAC)
Dahn, C., et al. 2002, AJ, 124, 1170
D'Antona, F., & Mazzitelli, I. 1997, Mem. Soc. Astron. Italiana, 68, 807
de Geus, E. J. 1992, A&A, 262, 258
de Zeeuw, P. T., Hoogerwerf, R., de Bruijne, J. H. J., Brown, A. G. A., & Blaauw, A. 1999, AJ, 117, 354
Dolidze, M. V., & Arakelyan, M. A. 1959, Soviet Astron., 3, 434
Edwards, S., Cabrit, S., Strom, S., Heyer, I., Strom, K., & Anderson, E. 1987, ApJ, 321, 473
Elias, J. H. 1978, ApJ, 224, 453
Feigelson, E. D. 1996, ApJ, 468, 306
Festin, L. 1998, A&A, 336, 883
Gagné, M., Skinner, S. L., & Daniel, K. J. 2004, ApJ, 613, 393
Grasdalen, G. L., Strom, K. M., & Strom, S. E. 1973, ApJ, 184, L53
Greene, T. P., & Meyer, M. R. 1995, ApJ, 450, 233
Greene, T. P., & Young, E. T. 1992, ApJ, 395, 516
Grosso, N., Montmerle, T., Bontemps, S., André, P., & Feigelson, E. D. 2000, A&A, 359, 113
Hartigan, P. 1993, AJ, 105, 1511
Hartmann, L., Hewett, R., & Calvet, N. 1994, ApJ, 426, 669
Hawley, S., et al. 2002, AJ, 123, 3409
Hillenbrand, L. A. 1997, AJ, 113, 1733
Hillenbrand, L. A., & White, R. J. 2004, ApJ, 604, 741
Imanishi, K., Koyama, K., & Tsuboi, Y. 2001, ApJ, 557, 747
Kirkpatrick, J. D., Henry, T. J., & McCarthy, D. W. 1991, ApJS, 77, 417
Lada, C. J., & Wilking, B. A. 1984, ApJ, 287, 610
Landolt, A. U. 1992, AJ, 104, 340
Leous, J. A., Feigelson, E. D., André, P., & Montmerle, T. 1991, ApJ, 379, 683
Livingston, W. C. 1999, in Allen's Astrophysical Quantities, ed. A. Cox (4th ed.; New York: AIP), 341
Loren, R. B. 1989, ApJ, 338, 925
Luhman, K. L. 1999, ApJ, 525, 466
Luhman, K. L., Liebert, J., & Rieke, G. H. 1997, ApJ, 489, L165
Luhman, K. L., & Rieke, G. H. 1999, ApJ, 525, 440
Martín, E. L., Montmerle, T., Gregorio-Hetem, J., & Casanova, S. 1998, MNRAS, 300, 733
Montmerle, T., Koch-Miramonde, L., Falgarone, E., & Grindlay, J. E. 1983, ApJ, 269, 182
Muzerolle, J., Calvet, N., & Hartmann, L. 2001, ApJ, 550, 944
Natta, A., Testi, L., Comerón, F., D'Antona, F., Baffa, C., Comoretto, G., & Gennari, S. 2002, A&A, 393, 597
Ozawa, H., Grosso, N., & Montmerle, T. 2005, A&A, 429, 963
Phelps, R. L., & Barsony, N. 2004, AJ, 127, 420
Preibisch, T., Brown, A. G. A., Bridges, T., Guenther, E., & Zinnecker, H. 2002, AJ, 124, 404
Preibisch, T., Guenther, E., & Zinnecker, H. 2001, AJ, 121, 1040
Preibisch, T., & Zinnecker, H. 1999, AJ, 117, 2381
Reipurth, B., & Clarke, C. 2001, AJ, 122, 432
Reipurth, B., Pedrosa, A., & Lago, M. T. V. T. 1996, A&AS, 120, 229
Rydgren, A. E. 1980, AJ, 85, 438
Schmidt-Kaler, Th. 1982, in Landolt-Bornstein New Series, Numerical Data and Functional Relationships in Science and Technology, Group 4, Vol. 2b, ed. K. Schaffers & H. H. Voigt (Springer: New York), 451
Sterzik, M. F., & Durisen, R. H. 1995, A&A, 304, L9
Struve, O., & Rudkjøbing, M. 1949, ApJ, 109, 92
Torres-Dodgen, A. V., & Weaver, W. B. 1993, PASP, 105, 693
Vrba, F. J., Strom, S. E., & Strom, K. M. 1976, AJ, 81, 958
Vrba, F. J., Strom, S. E., Strom, K. M., & Grasdalen, G. L. 1975, ApJ, 197, 77
Wilking, B. A., Greene, T. P., & Meyer, M. R. 1999, AJ, 117, 469 (WGM99)
Wilking, B. A., & Lada, C. J. 1983, ApJ, 274, 698
Wilking, B. A., Lada, C. J., & Young, E. T. 1989, ApJ, 340, 823
Wilking, B. A., Schwartz, R. D., & Blackwell, J. H. 1987, AJ, 94, 106
Wilking, B., Schwartz, R. D., Fanetti, T., & Friel, E. 1997, PASP, 109, 549